bioRxiv preprint doi: https://doi.org/10.1101/137307; this version posted May 12, 2017. The copyright holder for this preprint (which was not certified by peer review) is the author/funder, who has granted bioRxiv a license to display the preprint in perpetuity. It is made available under aCC-BY 4.0 International license.

DNA damage checkpoint dynamics drive cell cycle phase transitions

Hui Xiao Chao[1,2], Cere E. Poovey[1], Ashley A. Privette[1], Gavin D. Grant[3,4], Jeanette G. Cook[3,4], and Jeremy E. Purvis[1,2,4,†]

[1]Department of Genetics
[2]Curriculum for Bioinformatics and Computational Biology
[3]Department of Biochemistry and Biophysics
[4]Lineberger Comprehensive Cancer Center

University of North Carolina, Chapel Hill
120 Mason Farm Road
Chapel Hill, NC 27599-7264

[†]Corresponding Author:
Jeremy Purvis
Genetic Medicine Building 5061, CB#7264
120 Mason Farm Road
Chapel Hill, NC 27599-7264
jeremy_purvis@med.unc.edu

ABSTRACT

DNA damage checkpoints are cellular mechanisms that protect the integrity of the genome during cell cycle progression. The prevailing paradigm of DNA damage checkpoints is that they halt cell cycle progression until the damage is repaired, allowing cells time to recover from damage before resuming normal proliferation. Here, we challenge this model by observing cell cycle phase transitions in individual proliferating cells responding to acute DNA damage under live imaging conditions. We find that in gap phases (G1 and G2), DNA damage triggers an abrupt halt to cell cycle progression in which the length of arrest correlates with the severity of damage. However, cells that have already progressed beyond a proposed “commitment point” within a given cell cycle phase readily transition to the next phase, revealing a relaxation of checkpoint stringency during later stages of certain cell cycle phases. In contrast, cell cycle progression in S phase is significantly less sensitive to DNA damage. Instead of exhibiting a complete halt to cell cycle progression, our results are consistent with high DNA damage doses causing a decreased rate of progression. These phase-specific differences in DNA damage checkpoint dynamics lead to corresponding differences in the proportions of irreversibly arrested cells. Thus, the precise timing of DNA damage determines the sensitivity, rate of progression, and functional outcome of DNA damage checkpoints. These findings both explain and inform our understanding of cell fate decisions after treatment with common cancer therapeutics such as genotoxins or spindle poisons, which often target cells in a specific cell cycle phase.

bioRxiv preprint doi: https://doi.org/10.1101/137307; this version posted May 12, 2017. The copyright holder for this preprint (which was not certified by peer review) is the author/funder, who has granted bioRxiv a license to display the preprint in perpetuity. It is made available under aCC-BY 4.0 International license.

INTRODUCTION

The human cell cycle is a complex sequence of molecular events by which cells replicate and segregate their genomic DNA. Cell cycle progression is restrained by multiple checkpoint mechanisms that block transitions between cell cycle phases when cells encounter stressful conditions. For example, DNA damage activates checkpoints that delay cell cycle progression and trigger DNA repair. Under severe stress, DNA damage checkpoints may trigger permanent cellular outcomes such as apoptosis or senescence. Failure to fully activate DNA damage checkpoints can lead to genome instability, as the unrepaired DNA damage can be passed on to the next generation of cells[1–3]. On the other hand, because cells routinely experience low levels of endogenous DNA damage[4,5], timely checkpoint recovery after DNA damage repair is necessary for continued cell proliferation[6]. Therefore, the balance between cell cycle arrest and recovery must be regulated to continue proliferation in the face of constant exposure to endogenous and exogenous DNA damage sources.

It is generally viewed that activation of a DNA damage checkpoint arrests cell cycle progression to allow time for DNA repair, and that checkpoint-arrested cells eventually resume proliferation only after repair is complete[7–9]. However, the precise timing of events during the checkpoint response is not clear. For example, it is not known how abrupt the pause is; whether the pause is a complete halt or a graded reduction in cell cycle progression; or how the duration of the pause changes in response to different DNA damage doses and during different cell cycle phases. These variables could lead to differences in checkpoint stringency (which we defined as the robustness of cell cycle arrest by DNA damage) and affect the functional outcome for the cell. Knowledge of these collective dynamical behaviors—which we refer to as DNA damage checkpoint dynamics—is necessary for understanding the relationship between the DNA damage response and functional outcomes. It is also important for understanding the cellular consequences of many chemotherapeutic drugs, which act mainly by inducing DNA damage and interfering with cancer cell proliferation.

Among various forms of DNA damage, DNA double strand breaks (DSBs) are one of the most harmful types of lesions[10,11]. DSBs can give rise to chromosome rearrangements and deletions, which can subsequently lead to cancer. The functional effects of DSBs can vary depending on a cell's cell cycle phases. For example, it has long been known that cells in different cell cycle phases show drastic differences in survival under the same levels of ionizing radiation (which induces DSBs)[12]. The underlying basis for these differences in cell survival is not clear. One explanation for the observed differences in survival among the cell cycle phases is that each phase executes a unique DNA damage checkpoint mechanism. Indeed, the concept of distinct DNA damage checkpoint mechanisms at different stages of the cell cycle, such as G1/S, intra-S, and G2/M, has long existed. Precisely where within each cell cycle phase these checkpoints are interrupting cell cycle progression, however, is not clear and requires real-time analysis of DNA damage checkpoint dynamics. Thus, a quantitative understanding of DNA damage checkpoint dynamics is crucial to linking the molecular pathways to predicted cell cycle outcomes. This knowledge would not only help explain the difference in cell viabilities in response to DNA damage in different cell cycle phases but would greatly inform efforts to predict clinical outcomes of genotoxic chemotherapies, which often target cells in a specific cell cycle phase.

bioRxiv preprint doi: https://doi.org/10.1101/137307; this version posted May 12, 2017. The copyright holder for this preprint (which was not certified by peer review) is the author/funder, who has granted bioRxiv a license to display the preprint in perpetuity. It is made available under aCC-BY 4.0 International license.

Here, we use fluorescence time-lapse microscopy to reveal the dynamics of DNA damage checkpoints for three major phases—G1, S, and G2—by monitoring cell cycle progression upon acute DNA damage in otherwise unperturbed, asynchronously-dividing single cells. In response to DSBs, each cell cycle phase shows distinct DNA damage checkpoint dynamics. The G1 checkpoint employs a complete halt at high DNA damage levels but is more permissive to DNA damage than G2 because the checkpoint is temporally located well before the G1/S boundary. The S phase checkpoint is the least sensitive to DNA damage and does not completely halt cell cycle progression, but rather continuously slows the rate of progression throughout the remaining duration of S phase. The most stringent checkpoint occurs during G2/M, which abruptly and completely halts cell cycle progression by imposing a delay that is linearly correlated with the amount of DNA damage. Because of the internally located checkpoint in G1 and the graded slowdown of cell cycle progression in S phase, we found that the functional outcomes of DNA damage checkpoints can have a strong dependence on the timing of damage within each cell cycle phase. Taken together, our results argue that the timing of DNA damage relative to cell cycle phases and the time within each phase determine the sensitivity, dynamics, and functional outcome of checkpoint responses.

RESULTS

An “arrest-and-restart” model for DNA damage checkpoint regulation of cell cycle progression

DNA damage checkpoint regulation is a dynamic process that needs to adapt to changing environments. Checkpoint behavior must also include a fine-tuned balance between activation and inactivation to prevent lethal consequences of DNA DSBs and allowing proliferation to resume. Based on our current understanding of checkpoint mechanisms, checkpoints for DSBs are located at the G1/S, intra-S, or G2/M boundaries[13]. When damage occurs, checkpoint mechanisms completely halt cell cycle progression until the damage is repaired (**Figure 1A**). For asynchronously proliferating cells that experience DNA damage at different times during a given cell cycle phase, DNA damage checkpoint dynamics can be visualized by a “transition curve” that captures the rate of transition through cell cycle phases. To be precise, a transition curve plots the cumulative percentage of cells that transition into the next cell cycle phase against the post-damage transition time—the interval duration between the time of damage and the moment of transition into the next phase (**Figure 1B**). The plateau in each transition curve represents the time at which nearly all cells have successfully transitioned to the next phase.

Under the conventional DNA damage checkpoint model, there are two parameters that may vary in response to DNA damage levels. First, the duration of the cell cycle delay can lengthen with increasing amount of DNA damage. This corresponds to a rightward shift of the transition curve (**Figure 1C**). Second, when the damage is too excessive to be repaired, a cell may exit the cell cycle and enter permanent cell cycle arrest. As increasing levels of DNA damage increase the number of cells entering permanent arrest, the transition curve plateau lowers (**Figure 1D**). Under this model, cells may cope with increasing amounts of damage either by lengthening the duration of a temporary arrest, increasing the probability of entering permanent arrest, or both. Importantly, by analyzing an asynchronous cell population, one can gain insight into the dependency of DNA

bioRxiv preprint doi: https://doi.org/10.1101/137307; this version posted May 12, 2017. The copyright holder for this preprint (which was not certified by peer review) is the author/funder, who has granted bioRxiv a license to display the preprint in perpetuity. It is made available under aCC-BY 4.0 International license.

damage checkpoint sensitivity on the precise time within a cell cycle phase, since the damage is essentially randomly induced along the entire cell cycle phase. For example, in the case of damage level-dependent delay, as in Figure 1C, the same amount of damage causes a fixed delay duration independent of the timing of damage within the cell cycle phase (**Figure 1E**, left panel). When in a cell cycle phase whose early part is more sensitive to damage, cells that are damaged during early phase are arrested for longer durations than cells damaged near the end of the phase, resulting in a less steep transition curve. (**Figure 1E**, middle panel). Similarly, a cell cycle phase that has a more sensitive end phase corresponds to steeper transition curves (**Figure 1E**, right panel).

Quantification of cell cycle progression in individual, asynchronously proliferating cells

To test whether cells employ a dose-dependent arrest duration or a dose-dependent permanent arrest, we developed a fluorescent reporter system that allows real-time monitoring of cell cycle phase transitions in individual proliferating cells. Our goal was to quantify the duration of time a cell spends in G1, S, and G2/M. These three durations were quantified by recording 4 time points for each cell: the beginning of the cell cycle, the onset of S-phase, the end of S-phase, and the end of the cell cycle (**Figure 2A**). The beginning and end of each cell cycle was recorded as the time of cytokinesis of the mother cell and the time of cytokinesis of the given cell[14]. These two measurements indicate the total cell cycle duration for each cell. To determine the beginning and end of S-phase, we developed a modified reporter for S phase progression by fusing the red fluorescence protein mCherry to the proliferating cell nuclear antigen (PCNA) (PCNA-mCherry; **Figure 2B**). Multiple studies have shown that PCNA exhibits distinct punctate localization patterns at specific times within S-phase (e.g. sub-phases), and PCNA returns to diffuse nuclear localization upon exit from S[15–20].

We stably expressed the PCNA-mCherry reporter in both retinal pigmented epithelial (RPE-1 hTERT, abbreviated RPE) cells and in the osteosarcoma cell line U2OS. RPE cells are non-transformed human epithelial cells immortalized with telomerase reverse transcriptase with intact checkpoints, whereas U2OS cells are transformed cancer cell line which have an attenuated p53 response and an unstable G1 checkpoint due to p16 deficiency[21–23]. We imaged freely-proliferating cells through multiple cell divisions without affecting the cell cycle distribution properties (**Figure S1A**) or the cell cycle length (**Figure S1B**) as measured through flow cytometry and a traditional cell counting approach, respectively. These controls indicate that time-lapse imaging did not significantly alter cell cycle progression. As expected, we found that PCNA-mCherry formed replicative foci that appeared abruptly at the onset of S-phase and disappeared abruptly at the end of S-phase during the transition to G2 (**Figure 2C**). The emergence of PCNA-mCherry foci correlated strongly with EdU incorporation, while cells in other phases showed diffuse nuclear fluorescence (**Figure 2D-E**). This pattern of foci accumulation reliably identified the beginning and end of S-phase with 15-minute precision (**Figure 2E-F**). Thus, we established a system that quantifies, for individual cells, the duration of time spent in G1, S, G2/M, and, thus, the entire cell cycle.

Each cell cycle phase displays distinct DNA damage checkpoint dynamics

bioRxiv preprint doi: https://doi.org/10.1101/137307; this version posted May 12, 2017. The copyright holder for this preprint (which was not certified by peer review) is the author/funder, who has granted bioRxiv a license to display the preprint in perpetuity. It is made available under aCC-BY 4.0 International license.

With this reporter system in place, we experimentally determined DNA damage checkpoint dynamics for each cell cycle phase in individual RPE and U2OS cells. We induced DSBs in asynchronously dividing cells using the radiomimetic drug neocarzinostatin (NCS) and recorded the cell cycle phase in which the damage occurred. Confirming that NCS induced similar numbers of DSBs in each cell cycle phases (**Figure S2**) without affecting the PCNA-mCherry reporter's accuracy (**Figure S3**), we then followed each treated cell and measured the time until that cell exited its current cell cycle phase and transitioned to the next cell cycle phase. This analysis produced a transition curve for each dose of NCS and cell cycle phase (**Figure 3**, solid lines). With no external stress, nearly all of the RPE and U2OS cells transitioned to the next phase (>99%). As the dose of NCS was increased, however, two effects were observed. First, for cells damaged in G1 (**Figure 3A, 3D**) or G2/M (**Figure 3C, 3F**), increasing NCS concentrations reduced the number of cells that completed transitions within the 48-hour observation window, indicating a dose-dependent increase in the permanent arrest probability. Secondly, high DNA damage doses increased the time delay before half of the phase transitions occurred, particularly for cells damaged in G2/M (**Figure 3C, 3F**), indicating a dose-dependent increase in delay duration.

Several additional interesting observations emerged from these transition curves. In both RPE cells, which had a functional G1 checkpoint, and U2OS cells, which have an unstable G1 checkpoint[21,22], the transition curves exhibited a hyperbolic shape without an immediate delay (**Figure 3A, 3D**). Surprisingly, cells damaged during S phase transitioned to G2 without interruption for all but the highest NCS levels (**Figure 3B, 3E**), indicating a low sensitivity of the S phase checkpoint to DSBs. The few S-phase transition curves that did show a response to NCS also showed a hyperbolic shape similar to the G1 cells. In addition, almost all RPE and U2OS cells (>99%) damaged during S phase with the highest NCS concentrations were permanently arrested in the subsequent G2/M phase, with comparable or even higher arrest probabilities than cells damaged in G2/M with other NCS concentrations (**Figure S4**), suggesting that cells relied on the G2/M checkpoint to prevent catastrophic consequences of DNA damage incurred during S phase. In sharp contrast, cells damaged in G2 or M showed a sigmoidal transition curve with an immediate delay (**Figure 3C, 3F)**. Although the molecular pathways of the DNA damage response in each cell cycle phase show redundant mechanisms[9], these results suggest that each phase employs distinct checkpoint dynamics.

To explain these complex dynamics within our model framework, we fit our experimental data with the "arrest-and-restart" checkpoint model presented in **Figure 1A**. The model has two adjustable parameters: the duration of the cell cycle halt, and the percentage of cell entering permanent arrest (**Figure 3**, dashed lines, **Table S1** for fitted parameters, See **Supplementary Materials** and **Figure S5**). Although the model reproduced some features of the transition curves, there were significant discrepancies between the model fits and the data, suggesting that important features of the DNA damage checkpoints were not captured by the "arrest-and-restart" checkpoint model outlined in **Figure 1A**. For example, cells damaged in G1 transitioned to S phase at the same rate as unstressed cells until ~3 hours after damage, at which point the transition curve began to flatten. This initial rise in transition curves was also observed in G2/M for the first ~1 hour after damage. This behavior could be explained by a checkpoint commitment point that was temporally located 1~3

bioRxiv preprint doi: https://doi.org/10.1101/137307; this version posted May 12, 2017. The copyright holder for this preprint (which was not certified by peer review) is the author/funder, who has granted bioRxiv a license to display the preprint in perpetuity. It is made available under aCC-BY 4.0 International license.

hours before the end of the phase. Cells that have passed such a DNA damage "commitment point" are already irreversibly committed to transitioning at the time of damage despite triggering the DNA damage response (DDR). A second feature of the data that was not well captured by the model was the parabolic shape of the curves observed in G1 and S phases, which often showed gradual rightward shifts at the 50% transition point (e.g., **Figure 3B, 3D**). These features could be explained by a slowing down—rather than a complete halt—of cell cycle progression when the checkpoint was activated by DNA damage.

A refined model of DNA damage checkpoint regulation of cell cycle progression

In gap phases, DNA damage checkpoints are typically described acting primarily at the at the G1/S or G2/M boundaries[9,13], imposing a tight checkpoint that prevents cells with significant DNA damage from entering the next cell cycle phase (**Figure 1A**). In these descriptions, DNA damage can block transition to the next phase regardless of when the damage occurred. Our results prompted us to consider the possibility of a commitment point located at some internal point of a cell cycle phase after which DNA damage does not prevent the next transition. The exact temporal location of the proposed "commitment point" remains unclear, however. For example, a commitment point could exist at the phase-phase boundaries, resulting in arrest essentially regardless of when the damage occurs (**Figure 4A**, upper axis). Alternatively, the commitment point may be located somewhere internal to the cell cycle phase (**Figure 4A,** lower axis, example illustrating located at last 20% before entering the next phase). In the latter case, once a cell passes this point, it would not be subject to arrest by a DNA damage checkpoint in that phase, (but would presumably affect progression through the next phase). Moreover, we also allow that the cellular consequence of the checkpoint activation may not lead to a complete halt of cell cycle progression, which we refer to as "all-or-none" checkpoint activation (**Figure 4B**, upper axis). Instead, the checkpoint enforcement could be a partial slowdown of cell cycle progression that adjusts the *rate* of cell cycle progression relative to the extent of DNA damage level. We refer to this model of checkpoint enforcement as having "graded slowdown" kinetics (**Figure 4B**, lower axis). The above two modification can affect the transition curves: an internal commitment point would be expected to lead to a delay in the divergence of the transition curves of different DNA damage doses (**Figure 4C**); the graded slowdown checkpoint kinetics would lead to a decrease slope in the transition curves (**Figure 4D**).

To distinguish among these possibilities, we sought evidence of an internally located commitment point as well as checkpoint enforcement through graded slowdown kinetics. Computational simulations revealed a qualitative difference in the transition dynamics under different DNA damage checkpoint models (**Figure S6,** Supplementary Material). For checkpoints that triggered an abrupt and complete halt, the transition curves exhibited a sigmoidal shape with an immediate delay in transition right after damage, as seen in G2/M (**Figure S6A**). In contrast, under the graded slowdown model, where cells partially slowed down their progression in response to DNA damage, the transition curves were hyperbolic (**Figure S6B**), as seen mostly in S phase and sometime in G1. Furthermore, simulations that incorporated the internal checkpoint location revealed a delay in

bioRxiv preprint doi: https://doi.org/10.1101/137307; this version posted May 12, 2017. The copyright holder for this preprint (which was not certified by peer review) is the author/funder, who has granted bioRxiv a license to display the preprint in perpetuity. It is made available under aCC-BY 4.0 International license.

divergence of the curves under both checkpoint models (**Figure S6C-D**, compare red to other lines) as seen, for example, in the G1→S transition for both RPE and U2OS cells (**Figure 3A, 3G**).

We then fit our experimental data to the refined model (**Figure 4E-J**, **S7, Table S2-3**, see Supplementary Materials). For G1 in RPE and G2/M in both cell types, the data were consistent with all-or-none checkpoint kinetics. In addition, both G1 and G2/M showed evidence of internally located commitment points. For RPE cells, we estimated the commitment point location to be ~60% of the full G1 duration and ~30% for U2OS cells. These discrepancies could be related to the less stringent G1 arrest mechanisms thought to exist in U2OS cells[21,22]. For the combined G2/M phases, we detected commitment point at 80% and 90% of the full G2/M duration for RPE and U2OS, respectively. Since entry into M-phase is known to temporarily silence the DDR[24–29], this temporal position likely corresponds to the G2/M boundary, which was not precisely resolved in our system. For S phase cells, however, the graded slowdown checkpoint kinetics produced a better fit for both RPE and U2OS, with the commitment point located at 97% and 90% of S phase, respectively. Altogether, our results suggested that cells in G1 under high damage levels and all cells in G2/M implemented an all-or-none checkpoint activation whereas checkpoint responses in S phase showed graded slowdown kinetics. Furthermore, the G1 commitment point was located well before the G1/S boundary. In addition, in agreement with the “arrest-and-restart” model predictions, the refined model predicted that the halt duration in G2/M and the permanent arrest probability in gap phases increase with the level of DNA damage (**Figure S8**).

G1 and G2 checkpoints abruptly and completely halt cell cycle progression

We next sought to verify the predictions of our refined DNA damage checkpoint model. Specifically, the model predicts a dose-dependent halt duration in phases that display all-or-none checkpoint activation such as G1 under high damage level or G2/M. It also predicts that these checkpoints are enforced at an internally located commitment points. This would presumably lead to two populations of cells depending on the timing of DNA damage: cell damaged before the commitment point should be equally delayed in phase progression regardless of when the damage occurs, whereas cells damaged after the commitment point should proceed to the next phase without delay. In contrast, the model predicts that cells damaged in S phase should partially slow down their transition to G2 in proportion to the amount of damage. We examined the distributions of post-damage transition time in the three cell cycle phases, which showed evidence of two distinct checkpoint kinetics (**Figure 5**). Indeed, where our models predicted an all-or-none checkpoint (G1 and G2), we also observed distinct gaps in post-damage transition times (**Figure 5A, 5C**). This gap was most dramatic in G2/M, suggesting a checkpoint that imposed a stringent time delay in response to DNA damage; all cells that had passed the commitment point arrested for a substantial time. In contrast, cell damaged during S phase showed continuous distributions of post-damage transition times without any obvious gaps, consistent with the model’s prediction of graded slowdown checkpoint dynamics (**Figure 5B**). We thus concluded that our refined model capture many of the DNA damage response dynamics displayed by proliferating cells.

bioRxiv preprint doi: https://doi.org/10.1101/137307; this version posted May 12, 2017. The copyright holder for this preprint (which was not certified by peer review) is the author/funder, who has granted bioRxiv a license to display the preprint in perpetuity. It is made available under aCC-BY 4.0 International license.

We next characterized the checkpoint kinetics with respect to the arrest durations. Because the G2/M checkpoint provided the strongest evidence of a stringent, complete halt with a late and consistent commitment point, we focused our studies on the G2/M arrest kinetics.

The model predicted that the commitment point locations for G2/M were relatively close to the end of the combined G2/M phase (80% for RPE and 90% for U2OS). Consistent with the model prediction, we noticed only a small population (19% for RPE; 6% for U2OS) of G2/M cells that escaped the checkpoint and divided immediately after the highest 2 levels of NCS treatment (**Figure 5C**). These sub-populations that divided soon after DNA damage likely represent cells that had already entered mitosis, since the entry into mitosis has been shown to temporarily inactivate the DDR[9,26–28,30]. Indeed, based on the average G2/M durations for RPE (3.9hrs) and U2OS (6.5hrs) (**Figure S5**), the model predicted the checkpoint location to be ~0.7-0.8hr before cytokinesis. Since the average M phase consistently lasted approximately 40 mins based on nuclear envelope breakdown revealed by differential interference contrast images (**Figure S9**), the predicted commitment point location coincided with the G2/M boundary. Because the DNA damage checkpoint response had to be activated before reaching the G2/M boundary, this indicates that the checkpoint delays observed in our data were enforced entirely within G2 and not M phase. We therefore refer to this checkpoint as simply the G2 checkpoint henceforth.

The G2 checkpoint may impose a constant time delay upon a threshold level of DNA damage, or it may be programmed to calibrate the delay durations according to DNA damage levels, as suggested by the model fitting (**Figure S8A-B**). To distinguish between these possibilities, we examined the time gap between the onset of acute DNA damage and the next transition time point. We found the time delay was prolonged with increasing NCS concentration (**Figure 5C**), in linear proportion to the level of DSB incurred (**Figure S10**). Furthermore, the arrest durations were independent of when during G2 the cells were damaged (**Figure S11**). Together, these results suggested that the entire G2 phase was under the protection of DNA damage checkpoint. In response to acute DNA damage, the G2 checkpoint abruptly imposed a time delay that was proportional to the level of damage and independent of the progression stage of G2 phase.

The graded slowdown and non-terminal commitment point location link cell cycle outcome to cell cycle stage.

Our findings thus far indicate that each cell cycle phase has distinct DNA damage checkpoint kinetics and commitment locations. Although the two mechanisms are distinct, both the internal checkpoint location and the graded slowdown models predict that an individual cell's transition kinetics depend on the precise time that the cell experiences DNA damage. In the case of an internally located commitment point, DNA damage leads to arrest only when it occurs before the commitment point. In the case of a graded slowdown mechanism, cells that experience damage earlier during a phase would be expected to take longer to complete that phase since there is more remaining time subjected to the slowdown. We sought to test these predictions with further analyses of cells damaged at different times during each phase. We used asynchronously dividing cells

bioRxiv preprint doi: https://doi.org/10.1101/137307; this version posted May 12, 2017. The copyright holder for this preprint (which was not certified by peer review) is the author/funder, who has granted bioRxiv a license to display the preprint in perpetuity. It is made available under aCC-BY 4.0 International license.

damaged at different points during G1, S, and G2/M phases and plotted the total phase duration against the time already spent in that phase (**Figure 6A**).

To investigate the functional outcomes of these checkpoint responses, we categorized cells into three groups: unaffected (cells with total duration not significantly different from the control distribution), temporary arrest (cells with slowed progression but eventually transitioned by the end of the 48h experiment), and permanent arrest (cells that did not transition within 48 h) (**Figure 6B, S12**). Although transitions could potentially occur after 48h, most transitions took place during the first 35h with a small number of additional transitions afterwards (**Figure 5**), indicating statistically different responses between the transitioned and un-transitioned groups.

To access cell cycle outcomes from DNA damage in different cell cycle phases, we plotted the three categories of cell cycle outcomes as a dose response for each cell cycle phase (**Figure 6C-E, Figure S13**). Several interesting features emerged from this analysis. First, in all three phases, a smaller fraction of U2OS cells were affected by the same NCS concentrations compared to RPE, indicating a higher tolerance to DSBs as expected. Second, S phase cells had the highest NCS tolerance and responded only by temporary slowdown (**Figure 6D**). Third, in both G1 and G2, cells preferred temporary arrest response to low NCS levels, but changed to permanent arrest response to high NCS. Unlike during G1, when temporary arrest was never a predominant outcome (always <40%) and the change from temporary to permanent arrest was gradual (**Figure 6C**), G2 cells preferred temporary arrest in response to low NCS, but displayed a sharp switch to permanent arrest at ~ 40 ng/mL NCS in RPE and ~300 ng/mL in U2OS. The total fraction of affected cells (cells undergoing temporary or permanent arrest) was higher in G2 compared to G1 in both RPE and U2OS. Thus, the G2 checkpoint is overall the most stringent checkpoint, because fewer damaged cells escaped the checkpoint response. Altogether, the results suggested G1 and S phase checkpoints involve a gradual transition to permanent and temporary arrests, respectively, whereas the G2 checkpoint includes a sharp threshold above which cells switch to permanent arrest.

Finally, we asked whether cell cycle outcome depended on the timing of DNA damage *within* a cell cycle phase. Simulations revealed that, under the all-or-none model, the affected fraction was independent of cell cycle phase stage at the time of damage, as long as the damaged occurred before the commitment point (**Figure S14**, middle panels). In contrast, under the graded slowdown checkpoint model, the fraction of cells affected was inversely proportional to the progress into that phase at the time of damaged (**Figure S14**, right panels). Consistent with the model prediction, the total S phase durations were linearly and inversely correlated with the time spent in S phase before damage, with a slope consistent with the model predicted slowdown factors (**Figure S15**). This correlation also argued against the possibility that the decreased slope in S phase transition curves was due to the increased variations in halt duration with increased DNA damage level.

When we examined the cell cycle outcome's dependency on three stages of the cell cycle phase at time of damage (early, middle, and late), we noted consistent patterns: Cells damaged earlier during a phase were

bioRxiv preprint doi: https://doi.org/10.1101/137307; this version posted May 12, 2017. The copyright holder for this preprint (which was not certified by peer review) is the author/funder, who has granted bioRxiv a license to display the preprint in perpetuity. It is made available under aCC-BY 4.0 International license.

more likely to be affected than cells damaged later (**Figure 6F, Figure S16)**. The S phase checkpoint, which utilizes a graded slowdown checkpoint model, showed a linear decreasing affect as a function of time at the highest NCS concentration in RPE (**Figure 6F**, middle panel). In contrast, G2/M's early and middle stages, which presumably included only G2 cells, did not show a difference in arrest fraction, which was consistent with the abrupt all-or-none model (**Figure 6F**, right panel). The decreased fraction in the late stage was mostly due to M phase's insensitivity to DSBs. Therefore, this biphasic response in G2/M was characteristic of an all-or-none checkpoint model with a late restriction point. Importantly, G1 checkpoint outcome was inversely dependent on the stage progression (**Figure 6F**, left panel), consistent with a commitment point substantially earlier than the G1/S boundary.

DISCUSSION

Here, we used time-lapse fluorescent microscopy to study the dynamics of DNA damage checkpoints in asynchronously proliferating single human cells. Our analysis reveals that DNA damage checkpoint dynamics are cell cycle phase-specific (**Table 1**). Individual phases varied in several features: abruptness of the arrest response (all-or-none versus graded slowdown), the temporal location of an internal commitment point, and the types of functional responses (e.g., temporary versus permanent arrest).

The different checkpoint kinetics predicted by our model can be explained by the underlying biological mechanisms of each checkpoint. The transition from G1 to S phase is marked by the activation of DNA synthesis from multiple origins of DNA replication, an event that requires active Cyclin E/CDK2 and/or Cyclin A/CDK2[31,32]. The transition from G2 to M phase requires a large increase in cyclin B/CDK1 activity[33,34]. The all-or-none checkpoints we documented in both G1 in and G2 are consistent with switch-like mechanisms that inhibit the intracellular pools of cyclin/CDK complexes below their respective thresholds necessary for cell cycle transitions. These mechanisms involve molecular entities such as the CDK inhibitor p21 and Wee1-mediated CDK inactivation[35–37]. Without the corresponding cyclin-CDK complex activities essential to initiating DNA replication or mitosis, cell cycle progression through the G1/S and S/G2 transitions is blocked rather than simply slowed.

In contrast, the graded slowdown kinetics we documented in S phase is consistent with the intra-S checkpoint mediated inhibition of late-origin firing. Complete genome duplication is normally achieved by establishing replication forks at thousands of individual DNA replication origins, but some origins fire at the beginning of S phase whereas others fire later. When DNA damage is detected (typically by stalled replication forks), nearby otherwise "dormant" origins that have not yet fired initiate replication to promote replication completion in that local region. At the same time, checkpoint pathways block new origin firing in other regions of the genome corresponding to late-replicating domains[38,39]. Thus DNA synthesis continues at forks emanating from the early-fired origins, but the overall rate of S phase progression is slowed[40,41]. We postulate that this graded checkpoint response is protective to reduce the number of stalled replication forks that could collapse, snowballing the DNA damage[42]. Therefore, S phase actively counteracts the all-or-none mechanisms

bioRxiv preprint doi: https://doi.org/10.1101/137307; this version posted May 12, 2017. The copyright holder for this preprint (which was not certified by peer review) is the author/funder, who has granted bioRxiv a license to display the preprint in perpetuity. It is made available under aCC-BY 4.0 International license.

to avoid a prolonged stall with partially-replicated DNA, a situation that could lead to disastrous genome instability.

The location of the proposed commitment point can affect the apparent checkpoint stringency in a particular cell cycle phase. While both G1 and G2 utilize all-or-none checkpoint kinetics, the G2 checkpoint is more stringent than G1 in the sense that the commitment point occurs very close (within 0.5 h) to the G2/M border. In contrast, the G1 commitment point is located ~3-4 hours before the G1/S border in both RPE and U2OS, meaning that DNA damage within the last 3 hours of G1 fails to delay S phase onset. The earlier commitment point in G1 is consistent with previous observations that the G1 checkpoint fails to prevent S phase entry at early times after irradiation[43]. This longer damage-insensitive period in G1 versus G2 may be explained by differences in their biochemical pathways. In G1, the DNA damage response (DDR) involves transcriptional changes such as p53-dependent p21 induction[44,45], whereas DDR during G2 inactivates Cdc25, the rate-limiting step for CDK1 activation, through a faster series of phosphorylation and dephosphorylation reactions[46]. It is important to note that the commitment point that we describe is similar, but not identical, to the concept of a G1 restriction point, a temporal point at which cells in G1 are no longer sensitive to growth factor withdrawal for commitment to S phase entry[47]. Although mediated through different upstream mechanisms, the downstream consequences of serum starvation and DDR both converge on CDK2/4 inactivation[48]. Interestingly, the temporal location of the restriction point is comparable to the location of our G1 commitment point mapped 2-3 hours before DNA replication[49], suggesting that different types of cell cycle checkpoints in G1 may act on a similar timescale due to their converging pathways.

Previous studies that examine cell tolerance to DSBs, or radiosensitivity, measured by survival rate after irradiation, also exhibit drastic variation across different cell cycle phases. Specifically, G2 and M phase cells show the most sensitivity to radiation, followed by G1 cells, with S phase cells being the most resistant to damage[12]. Our results using a radiomimetic drug reveal a similar trend in checkpoint stringencies. The G2/M checkpoint is the most stringent whereas the S phase checkpoint is the least stringent. Therefore, the stringencies of DNA damage checkpoints in each phase seem to be optimized to allow for maximal cell cycle progression while preventing the lethal consequences of DSBs. Remarkably, S phase progression was minimally affected by damage except for extremely high NCS concentrations (**Figure 3B**). Even under the highest levels of damage, cells progressed through S phase and were rarely found to undergo permanent arrest. The fact that S phase shows the least stringent checkpoint yet is the most resistant to irradiation in terms of viability seems contradictory, since a robust DNA damage checkpoint would be expected to offer the strongest protection from irradiation. However, we found that cells damaged in S phase were arrested in the subsequent G2 phase by comparable or even higher probabilities than cells damaged directly during G2/M (**Figure S4**). This observation suggests that cells damaged in S phase carry incompletely repaired DSBs to G2 and then trigger a robust G2 checkpoint response that protects their viability. Therefore, therapeutically, it might be more effective to target S phase tumor cells when combined with checkpoint inhibitors of G2/M rather than inhibitors of S phase progression.

bioRxiv preprint doi: https://doi.org/10.1101/137307; this version posted May 12, 2017. The copyright holder for this preprint (which was not certified by peer review) is the author/funder, who has granted bioRxiv a license to display the preprint in perpetuity. It is made available under aCC-BY 4.0 International license.

Our work also demonstrates the advantage of using quantitative live-imaging approach to study cell cycle dynamics. Live-cell imaging measures DNA damage checkpoint dynamics under physiological conditions without artificial manipulations such as cell synchronization, which perturbs the cell cycle and can introduce unwanted DNA damage. Furthermore, our study also provides an accurate methodology for locating cell cycle transitions and commitment points. This method provides an advantage over the widely-used fluorescence ubiquitin cell cycle indicator (FUCCI) system[50–53], a quantitative ubiquitination-based fluorescence reporter that uses tagged Cdt1 and geminin fragments to report the G1 and S/G2/M phases in real time. Whereas the FUCCI system is only capable of segmenting the cell cycle into 2 phases—G1 and S/G2/M[50,51,53]—and is not capable of sharply demarcating the G1/S transition[52], the PCNA-based method provides a finer resolution demarking the boundaries at the G1/S and S/G2 borders[52]. This capability is crucial for precisely locating the proposed DNA damage commitment points relative to cell cycle phase boundaries. Another advantage of using PCNA as a marker of phase transition is its robustness to intensity fluctuation. In the FUCCI system, the demarcation of phase transitions relies on fluorescence intensity, which can vary under different imaging conditions, expression levels, and fluorophore degradation kinetics. In contrast, the phase identification by the PCNA reporter relies on morphological changes due to protein localization that are insensitive to total fluorescence intensity as well as the rates of fluorophore maturation and degradation. Thus, our results provide precise identification of the timing of cell cycle phase transitions after DNA damage.

Finally, our study reveals meaningful differences between an immortalized primary cell line and a transformed cell line derived from a human tumor. Despite qualitatively similar checkpoint dynamics observed within each phase between RPE and U2OS cells, we find quantitative differences in checkpoint stringencies—specifically, diminished checkpoint stringencies in the transformed U2OS cell lines across the cell cycle. This deficiency is most pronounced in G1, which has been shown to harbor an unstable G1 checkpoint due to p16 deficiency and p53 heterozygosity[21,22]. Our model predicts that the G1 checkpoint in U2OS employs a graded slowdown kinetic even with the highest DNA damage level induced, as opposed to the all-or-none kinetics seen in RPE cells. It is possible that this difference in checkpoint kinetics may reflect a more general discrepancy between non-transformed and cancer cells. The graded slowdown kinetics may explain the “leakiness” of DNA damage checkpoint observed in transformed cells, which has been loosely attributed to defective checkpoint responses[54,55]. Thus, in light of cancer treatments that rely on differentially inducing DNA damage, it may be useful to clinically stratify tumors not only based on cell types, but also on the dynamics of DNA damage checkpoint responses.

EXPERIMENTAL PROCEDURES

Cell culture

U2OS cells were obtained from the laboratory of Dr. Yue Xiong and cultured in McCoy’s 5A medium supplemented with 10% fetal bovine serum (FBS) and penicillin/streptomycin (Gibco). hTERT retinal pigment epithelial cells (RPE) were obtained from the ATCC (ATCC® CRL-4000™) and cultured in DMEM medium

bioRxiv preprint doi: https://doi.org/10.1101/137307; this version posted May 12, 2017. The copyright holder for this preprint (which was not certified by peer review) is the author/funder, who has granted bioRxiv a license to display the preprint in perpetuity. It is made available under aCC-BY 4.0 International license.

supplemented with 10% fetal calf serum and penicillin/streptomycin. When required, the medium was supplemented with selective antibiotics (2 µg/mL puromycin (Gibco)). When indicated, medium was replaced with fresh medium supplemented with 200 ng/mL neocarzinostatin (Sigma-Aldrich) during experiments. Clonogenic assay was performed using the CellTiter-Blue Cell Viability Assay (Promega). Cell cycle distributions were analyzed by DAPI staining and by incorporation of EdU using the Click-iT EdU kit (Invitrogen).

Cell Line Construction

The pLenti-PGK-Puro-TK-NLS-mCherry-PCNA plasmid was subcloned from eGFP-PCNA (Gift from S. Angus) using the Gateway system (Life Technologies) following manufacturers protocols. The eGFP tag from the original plasmid was replaced with mCherry in the pENTR vector intermediate using standard methods. pLenti PGK Puro DEST (w529-2) was a gift from Eric Campeau (Addgene plasmid # 19068)[56]. The plasmid was stably expressed into U2OS or RPE cells by first transfecting the plasmid into 293T cells to generate replication-defective viral particles using standard protocols (TR-1003 EMD Millipore), which were used to stably infect the U2OS and RPE cell lines. The cells were maintained in selective media and hand-picked to generate a clonal population.

Time-Lapse Microscopy

Prior to microscopy, cells were plated in poly-D-lysine coated glass-bottom plates (Cellvis) with FluoroBrite™ DMEM (Invitrogen) supplemented with FBS, 4 mM L-glutamine, and penicillin/streptomycin. Fluorescence images were acquired using a Nikon Ti Eclipse inverted microscope with a Nikon Plan Apochromat Lambda 40X objective with a numerical aperture of 0.95 using an Andor Zyla 4.2 sCMOS detector. In addition, we employed the Nikon Perfect Focus System (PFS) in order to maintain focus of live cells throughout the entire acquisition period. The microscope was surrounded by a custom enclosure (Okolabs) in order to maintain constant temperature (37°C) and atmosphere (5% CO_2). The filter sets used were CFP - 436/20 nm; 455 nm; 480/40 nm (excitation; beam splitter; emission filter), YFP - 500/20nm; 515 nm; 535/30 nm; and mCherry - 560/40 nm; 585 nm; 630/75 nm (Chroma). Images were acquired every 20 mins for U2OS cells and every 10 minutes for RPE cells in the YFP and mCherry channels. We acquired 2-by-2 stitched large image for RPE cell. NIS-Elements AR software was used for image acquisition and analysis.

Image Analysis

Image analysis was done by CellProfiler's customized pipeline that included speckle counting and object tracking[57], followed by Matlab (MathWorks) based custom written software. The image analysis algorithm was optimized to identify PCNA-mCherry foci that produced the PCNA foci trajectory. The tracking of cells was done manually using ImageJ.

In silico mapping of cell cycle progression in individual cells

bioRxiv preprint doi: https://doi.org/10.1101/137307; this version posted May 12, 2017. The copyright holder for this preprint (which was not certified by peer review) is the author/funder, who has granted bioRxiv a license to display the preprint in perpetuity. It is made available under aCC-BY 4.0 International license.

We quantified the cell cycle phase durations of our cell lines by imaging asynchronously dividing cells. During the entire life of each individual cell, we took four time point measurements: the time of cell birth (t_{birth}), the onset of S phase (t_{s_onset}), the end of S phase (t_{s_end}), and the time of cytokinesis ($t_{cytokinesis}$) (**Figure 2A**), which were manually identified from the PCNA-mCherry reporter. These four time points allowed for quantifying the durations of three major cell cycle phases: G1, S, and G2/M phases. For cells with exogenous DNA damage, prior to addition of NCS, we imaged freely cycling cells for at least 15 hours to establish the cell cycle phase duration before which the DNA damage was induced.

Immunofluorescence

Cells were fixed and permeabilized with -20°C methanol for 10 minutes, and stained overnight at 4°C with anti-phospho-H2AX Ser139 (JBW301, EMD Millipore 05-636). Primary antibodies were visualized using a secondary antibody conjugated to Alexa Fluor-488/-647 and imaged with appropriate filters. EdU incorporation and staining was performed using the Click-iT™ EdU kit (Invitrogen C10337).

ACKNOWLEDGEMENTS

We thank Yue Xiong for helpful discussion, Samuel Wolff for guidance on experiments and microscopy operation, Katarzyna Kedziora for critical feedback, and Po-Hao Huang for brainstorming ideas. This work was supported by National Institutes of Health research grants R00-GM102372 (JEP) and R01-GM102413 (JGC), National Institutes of Health training grants T32CA009156-40 (GDG) and T32GM067553-12 (HXC), the North Carolina University Cancer Research Fund, and by a medical research grant from the W. M. Keck Foundation (JEP and JGC).

AUTHOR CONTRIBUTIONS

HXC and GDG constructed the PCNA-mCherry reporter cell lines. HXC performed validation studies. HXC and JEP designed the experiments. HXC, CEP, and AAP performed live-cell imaging and experiments. HXC, CEP, and AAP conducted image analysis and cell tracking. HXC performed computational modeling and analysis. HXC wrote the manuscript with contributions from all authors.

CONTRIBUTIONS FIGURE LEGENDS

Figure 1. Model of DNA damage checkpoint dynamics

A. “Arrest-and-restart” model of cell cycle checkpoint dynamics in response to DNA damage. The green arrow represents unrestricted progression of a cell cycle phase through time. In the absence of DNA damage, cells

bioRxiv preprint doi: https://doi.org/10.1101/137307; this version posted May 12, 2017. The copyright holder for this preprint (which was not certified by peer review) is the author/funder, who has granted bioRxiv a license to display the preprint in perpetuity. It is made available under aCC-BY 4.0 International license.

progress readily through a phase with duration t_1. When damage occurs, progression through a phase is temporarily interrupted, resulting in an increase in phase duration, t_2.

B. Schematic of a transition curve. A transition curve is obtained by measuring the post-damage transition times of an asynchronous population of cells that are damaged at different points during a particular cell cycle phase. Each green arrow represents an individual cell's progression through a particular cell cycle phase. The transition curve plots the cumulative percentage of cells that have successfully transitioned to the next phase.

C. Transition curves expected from a graded halt duration response to DNA damage level. Increasing damage causes a corresponding delay before cells transition to the next cell cycle phase.

D. Transition curves expected from a graded permanent arrest response to DNA damage level. Increasing damage results in fewer cells transitioning to the next phase.

E. Expected transition curves when DNA damage sensitivity varies throughout a cell cycle phase. The intensity of grey arrows indicates the DNA damage sensitivity. Increased sensitivity during the early parts of a phase allows cells that are already near the end of the phase to transition more readily (middle plot). Greater sensitivity in the later part of a phase results in an immediate delay to transition of the population (right plot).

Figure 2. Quantification of cell cycle phase duration in single cells

A. Cell cycle diagram showing three phases—G1, S, and G2/M— defined by four measured time points.

B. Schematic showing the construct design for PCNA-mCherry reporter

C. Sequence of live cell images of U2OS cells expressing the PCNA-mCherry reporter.

D. Immunofluorescence (IF) staining for EdU incorporation in the reporter cell line. Cells expressing PCNA-mCherry were pulsed with 10 μM EdU for 1 hour, fixed, and stained for EdU and DAPI. White arrows indicate S phase cells with punctate PCNA pattern.

E. Live cell imaging combined with fixed-cell IF staining with EdU incorporation. Asynchronously cycling cells were imaged for 24 hours, and the number of PCNA foci in each cell was quantified every 15 mins. At the end of the movie, cells were pulsed with 10 μM EdU for 15 minutes, fixed, and quantified for EdU incorporation.

F. Method for S phase identification based on PCNA-mCherry foci trajectories. The plot shows a typical single-cell time series of PCNA foci number. The onset and the end of S phases were identified by the initial maximal increase and final maximal drop, respectively, in the number of PCNA foci.

Figure 3. Each cell cycle phase exhibits distinct DNA damage checkpoint dynamics.

A-C. Cell cycle phase-specific transition curves in response to acute DNA damage in RPE cells. *Upper panels and solid lines*: transition curves for asynchronously dividing RPE treated with NCS at the indicated concentrations during (A) G1, (B) S, or (C) G2/M. For each cell, we quantified the time interval between NCS treatment and the transition from its current cell cycle phase to the next phase. *Lower panels and dashed lines*: Best fit lines of the experimental data to the "arrest-and-restart" DNA damage checkpoint model described in **Figure 1A.**

D-F. Corresponding experimental data and model fits for U2OS cells as described in panels A-C.

bioRxiv preprint doi: https://doi.org/10.1101/137307; this version posted May 12, 2017. The copyright holder for this preprint (which was not certified by peer review) is the author/funder, who has granted bioRxiv a license to display the preprint in perpetuity. It is made available under aCC-BY 4.0 International license.

Figure 4. A refined model for DNA damage checkpoint dynamics that incorporates an internal commitment point and graded slowdown kinetics.

A. Schematic of models for variable DNA damage checkpoint location. The model incorporates a temporally located commitment point. Cells that are damaged after this time point transition to the next phase without arrest.

B. Schematic of models for DNA damage checkpoints with different kinetics. Upper panel: A checkpoint that is enforced in an all-or-none manner halts the cell cycle progression completely upon DNA damage. Lower panel: A checkpoint that is enforced by slowing down the rate of cell cycle progression upon DNA damage without completely halting the progression.

C. Expected transition curves under the model of a DNA damage checkpoint that is internally located. The initial increase in transition percentage for all damage levels represents the fraction of cells that were beyond the commitment point.

D. Expected transition curves under the graded slowdown kinetic checkpoint model. The change in slopes among different DNA damage levels results from differences in the time of damage for individual cells. Cells damaged earlier in the phase experience a longer delay.

E-J. Cell cycle phase-specific transition curves in response to acute DNA damage, as in Figure 3's lower panels, but fitted with the refined model that incorporated both the flexible checkpoint location and the possibility of graded slowdown checkpoint kinetics (S phase).

Figure 5. The G1 and G2 DNA damage checkpoints enforce a complete halt to cell cycle progression by an interval that is proportional to the damage level.

A. The post-damage G1→S transition time durations of cells damaged anytime during G1 in RPE (left panel) and U2OS (right panel) cells.

B. The post-damage S→G2 transition time durations of cells damaged anytime during S in RPE (left panel) and U2OS (right panel) cells.

C. The post-damage G2/M→G1 transition time durations of cells damaged anytime during G2 or M in RPE (left panel) and U2OS (right panel) cells.

Figure 6. Cell cycle outcomes depend on the timing of DNA damage both within and between cell cycle phases.

A. Schematic showing the definitions of time spent before damage, post-damage transition time, and total phase duration.

B. Classifying individual cells into three cell cycle outcomes based on phase duration. Here, we show U2OS cells treated during G2/M to demonstrate the classification strategy. Untreated cells (*left*) were used to identify a subpopulation of cells whose phase durations fell above the 95% percentile. These cells were considered to be arrested. (*right*) U2OS cells treated with 100ng/mL NCS during G2/M showing a large fraction of cells above the threshold identified in the control population.

bioRxiv preprint doi: https://doi.org/10.1101/137307; this version posted May 12, 2017. The copyright holder for this preprint (which was not certified by peer review) is the author/funder, who has granted bioRxiv a license to display the preprint in perpetuity. It is made available under aCC-BY 4.0 International license.

C-E. Phase-specific cell cycle outcomes in response to increasing doses of acute DNA damage. Error bars represents binomial standard error. Upper panels: RPE. Lower panels: U2OS

F. Dependency of cell cycle outcome on the stage of cell cycle phase progression. Representative cell cycle outcomes for each phase's checkpoint are plotted as a function of cell cycle phase stage—early, mid, or late stages. G1 and S phases are shown for RPE cells, which display more physiological checkpoint responses than U2OS cells. G2 phase is shown for U2OS cells because the RPE G2 duration was too short to be readily subdivided into stages. Cells were assigned to early, mid, or late stages based on whether the time they spent in that phase fell within the first, second, or third equal partition (tercile) of the theoretical distributions of time spent in each phase, respectively.

Table 1. Summary of checkpoint dynamics as a function of cell cycle phase

References

1. Nyberg, K. A., Michelson, R. J., Putnam, C. W. & Weinert, T. A. Toward Maintaining the Genome: DNA Damage and Replication Checkpoints. *Annu. Rev. Genet.* **36,** 617–656 (2002).

2. Löbrich, M. & Jeggo, P. A. The impact of a negligent G2/M checkpoint on genomic instability and cancer induction. *Nat. Rev. Cancer* **7,** 861–869 (2007).

3. Sogo, J. M., Lopes, M. & Foiani, M. Fork Reversal and ssDNA Accumulation at Stalled Replication Forks Owing to Checkpoint Defects. *Science (80-.).* **297,** (2002).

4. Vilenchik, M. M. & Knudson, A. G. Endogenous DNA double-strand breaks: production, fidelity of repair, and induction of cancer. *Proc. Natl. Acad. Sci. U. S. A.* **100,** 12871–6 (2003).

5. Haber, J. E. DNA recombination: the replication connection. *Trends Biochem. Sci.* **24,** 271–5 (1999).

6. Bartek, J. & Lukas, J. DNA damage checkpoints: from initiation to recovery or adaptation. *Curr. Opin. Cell Biol.* **19,** 238–245 (2007).

7. Wang, H., Zhang, X., Teng, L. & Legerski, R. J. DNA damage checkpoint recovery and cancer development. *Exp. Cell Res.* **334,** 350–358 (2015).

8. Paulovich, A. G., Toczyski, D. P. & Hartwell, L. H. When checkpoints fail. *Cell* **88,** 315–21 (1997).

9. Shaltiel, I. A. *et al.* The same, only different - DNA damage checkpoints and their reversal throughout the cell cycle. *J. Cell Sci.* **128,** 607–20 (2015).

10. Khanna, K. K. & Jackson, S. P. DNA double-strand breaks: signaling, repair and the cancer connection. *Nat. Genet.* **27,** 247–54 (2001).

bioRxiv preprint doi: https://doi.org/10.1101/137307; this version posted May 12, 2017. The copyright holder for this preprint (which was not certified by peer review) is the author/funder, who has granted bioRxiv a license to display the preprint in perpetuity. It is made available under aCC-BY 4.0 International license.

11. van Gent, D. C., Hoeijmakers, J. H. & Kanaar, R. Chromosomal stability and the DNA double-stranded break connection. *Nat. Rev. Genet.* **2,** 196–206 (2001).

12. Pawlik, T. M. & Keyomarsi, K. Role of cell cycle in mediating sensitivity to radiotherapy. *Int. J. Radiat. Oncol. Biol. Phys.* **59,** 928–42 (2004).

13. Finn, K., Lowndes, N. F. & Grenon, M. Eukaryotic DNA damage checkpoint activation in response to double-strand breaks. *Cell. Mol. Life Sci.* **69,** 1447–73 (2012).

14. Davis, D. M. & Purvis, J. E. Computational analysis of signaling patterns in single cells. *Semin. Cell Dev. Biol.* **37,** 35–43 (2015).

15. Kisielewska, J., Lu, P. & Whitaker, M. GFP-PCNA as an S-phase marker in embryos during the first and subsequent cell cycles. *Biol. Cell* **97,** 221–9 (2005).

16. Zölzer, F., Basu, O., Devi, P. U., Mohanty, S. P. & Streffer, C. Chromatin-bound PCNA as S-phase marker in mononuclear blood cells of patients with acute lymphoblastic leukaemia or multiple myeloma. *Cell Prolif.* **43,** 579–83 (2010).

17. Sporbert, A., Gahl, A., Ankerhold, R., Leonhardt, H. & Cardoso, M. C. DNA Polymerase Clamp Shows Little Turnover at Established Replication Sites but Sequential De Novo Assembly at Adjacent Origin Clusters. *Mol. Cell* **10,** 1355–1365 (2002).

18. Pomerening, J. R., Ubersax, J. A., Ferrell, J. E. & Jr. Rapid cycling and precocious termination of G1 phase in cells expressing CDK1AF. *Mol. Biol. Cell* **19,** 3426–41 (2008).

19. Leonhardt, H. Dynamics of DNA Replication Factories in Living Cells. *J. Cell Biol.* **149,** 271–280 (2000).

20. Essers, J. *et al.* Nuclear dynamics of PCNA in DNA replication and repair. *Mol. Cell. Biol.* **25,** 9350–9 (2005).

21. Diller, L. *et al.* p53 functions as a cell cycle control protein in osteosarcomas. *Mol. Cell. Biol.* **10,** 5772–81 (1990).

22. Stott, F. J. *et al.* The alternative product from the human CDKN2A locus, p14(ARF), participates in a regulatory feedback loop with p53 and MDM2. *EMBO J.* **17,** 5001–14 (1998).

23. Akan, P. *et al.* Comprehensive analysis of the genome transcriptome and proteome landscapes of three tumor cell lines. *Genome Med.* **4,** 86 (2012).

24. Jullien, D., Vagnarelli, P., Earnshaw, W. C. & Adachi, Y. Kinetochore localisation of the DNA damage response component 53BP1 during mitosis. *J. Cell Sci.* **115,** 71–9 (2002).

bioRxiv preprint doi: https://doi.org/10.1101/137307; this version posted May 12, 2017. The copyright holder for this preprint (which was not certified by peer review) is the author/funder, who has granted bioRxiv a license to display the preprint in perpetuity. It is made available under aCC-BY 4.0 International license.

25. Cesare, A. J. Mitosis, double strand break repair, and telomeres: a view from the end: how telomeres and the DNA damage response cooperate during mitosis to maintain genome stability. *Bioessays* **36,** 1054–61 (2014).

26. Orthwein, A. *et al.* Mitosis Inhibits DNA Double-Strand Break Repair to Guard Against Telomere Fusions. *Science (80-.).* **344,** 189–193 (2014).

27. Heijink, A. M., Krajewska, M. & van Vugt, M. A. T. M. The DNA damage response during mitosis. *Mutat. Res. Mol. Mech. Mutagen.* **750,** 45–55 (2013).

28. ZIRKLE, R. E. & BLOOM, W. Irradiation of parts of individual cells. *Science* **117,** 487–93 (1953).

29. Rieder, C. L. & Cole, R. W. Entry into Mitosis in Vertebrate Somatic Cells Is Guarded by a Chromosome Damage Checkpoint That Reverses the Cell Cycle When Triggered during Early but Not Late Prophase. *J. Cell Biol.* **142,** 1013–1022 (1998).

30. Mikhailov, A. *et al.* DNA damage during mitosis in human cells delays the metaphase/anaphase transition via the spindle-assembly checkpoint. *Curr. Biol.* **12,** 1797–806 (2002).

31. Labib, K. How do Cdc7 and cyclin-dependent kinases trigger the initiation of chromosome replication in eukaryotic cells? *Genes Dev.* **24,** 1208–1219 (2010).

32. Tanaka, S. & Araki, H. Helicase Activation and Establishment of Replication Forks at Chromosomal Origins of Replication. *Cold Spring Harb. Perspect. Biol.* **5,** a010371–a010371 (2013).

33. Taylor, W. R. & Stark, G. R. Regulation of the G2/M transition by p53. *Oncogene* **20,** 1803–1815 (2001).

34. Lindqvist, A., Rodríguez-Bravo, V. & Medema, R. H. The decision to enter mitosis: feedback and redundancy in the mitotic entry network. *J. Cell Biol.* **185,** 193–202 (2009).

35. Nigg, E. A. Mitotic kinases as regulators of cell division and its checkpoints. *Nat. Rev. Mol. Cell Biol.* **2,** 21–32 (2001).

36. Donzelli, M. & Draetta, G. F. Regulating mammalian checkpoints through Cdc25 inactivation. *EMBO Rep.* **4,** 671–677 (2003).

37. Reinhardt, H. C. & Yaffe, M. B. Kinases that control the cell cycle in response to DNA damage: Chk1, Chk2, and MK2. *Curr. Opin. Cell Biol.* **21,** 245–55 (2009).

38. Ge, X. Q. & Blow, J. J. Chk1 inhibits replication factory activation but allows dormant origin firing in existing factories. *J. Cell Biol.* **191,** 1285–1297 (2010).

39. Yekezare, M., Gomez-Gonzalez, B. & Diffley, J. F. X. Controlling DNA replication origins in response to DNA damage - inhibit globally, activate locally. *J. Cell Sci.* **126,** 1297–1306 (2013).

bioRxiv preprint doi: https://doi.org/10.1101/137307; this version posted May 12, 2017. The copyright holder for this preprint (which was not certified by peer review) is the author/funder, who has granted bioRxiv a license to display the preprint in perpetuity. It is made available under aCC-BY 4.0 International license.

40. Paulovich, A. G. & Hartwell, L. H. A checkpoint regulates the rate of progression through S phase in S. cerevisiae in response to DNA damage. *Cell* **82,** 841–7 (1995).

41. Tercero, J. A. & Diffley, J. F. X. Regulation of DNA replication fork progression through damaged DNA by the Mec1/Rad53 checkpoint. *Nature* **412,** 553–557 (2001).

42. Cortez, D. Preventing replication fork collapse to maintain genome integrity. *DNA Repair (Amst).* **32,** 149–57 (2015).

43. Deckbar, D. *et al.* The Limitations of the G1-S Checkpoint. *Cancer Res.* **70,** 4412–4421 (2010).

44. Macleod, K. F. *et al.* p53-dependent and independent expression of p21 during cell growth, differentiation, and DNA damage. *Genes Dev.* **9,** 935–44 (1995).

45. Waldman, T., Kinzler, K. W. & Vogelstein, B. p21 Is Necessary for the p53-mediated G1 Arrest in Human Cancer Cells. *Cancer Res.* **55,** (1995).

46. Donzelli, M. & Draetta, G. F. Regulating mammalian checkpoints through Cdc25 inactivation. *EMBO Rep.* **4,** 671–7 (2003).

47. Pardee, A. B. A Restriction Point for Control of Normal Animal Cell Proliferation. *Proc. Natl. Acad. Sci.* **71,** 1286–1290 (1974).

48. Blagosklonny, M. V. & Pardee, A. B. The Restriction Point of the Cell Cycle. *Cell Cycle* **1,** 102–109 (2002).

49. Campisi, J., Medrano, E. E., Morreo, G. & Pardee, A. B. Restriction point control of cell growth by a labile protein: evidence for increased stability in transformed cells. *Proc. Natl. Acad. Sci. U. S. A.* **79,** 436–40 (1982).

50. Saitou, T. & Imamura, T. Quantitative imaging with Fucci and mathematics to uncover temporal dynamics of cell cycle progression. *Dev. Growth Differ.* **58,** 6–15 (2016).

51. Dowling, M. R. *et al.* Stretched cell cycle model for proliferating lymphocytes. *Proc. Natl. Acad. Sci. U. S. A.* **111,** 6377–82 (2014).

52. Wilson, K. A., Elefanty, A. G., Stanley, E. G. & Gilbert, D. M. Spatio-temporal re-organization of replication foci accompanies replication domain consolidation during human pluripotent stem cell lineage specification. *Cell Cycle* 0 (2016). doi:10.1080/15384101.2016.1203492

53. Sandler, O. *et al.* Lineage correlations of single cell division time as a probe of cell-cycle dynamics. *Nature* **519,** 468–471 (2015).

bioRxiv preprint doi: https://doi.org/10.1101/137307; this version posted May 12, 2017. The copyright holder for this preprint (which was not certified by peer review) is the author/funder, who has granted bioRxiv a license to display the preprint in perpetuity. It is made available under aCC-BY 4.0 International license.

54. Kastan, M. B. *et al.* A mammalian cell cycle checkpoint pathway utilizing p53 and GADD45 is defective in ataxia-telangiectasia. *Cell* **71,** 587–597 (1992).

55. Bunz, F. *et al.* Requirement for p53 and p21 to Sustain G2 Arrest After DNA Damage. *Science (80-.).* **282,** (1998).

56. Campeau, E. *et al.* A Versatile Viral System for Expression and Depletion of Proteins in Mammalian Cells. *PLoS One* **4,** e6529 (2009).

57. Carpenter, A. E. *et al.* CellProfiler: image analysis software for identifying and quantifying cell phenotypes. *Genome Biol.* **7,** R100 (2006).

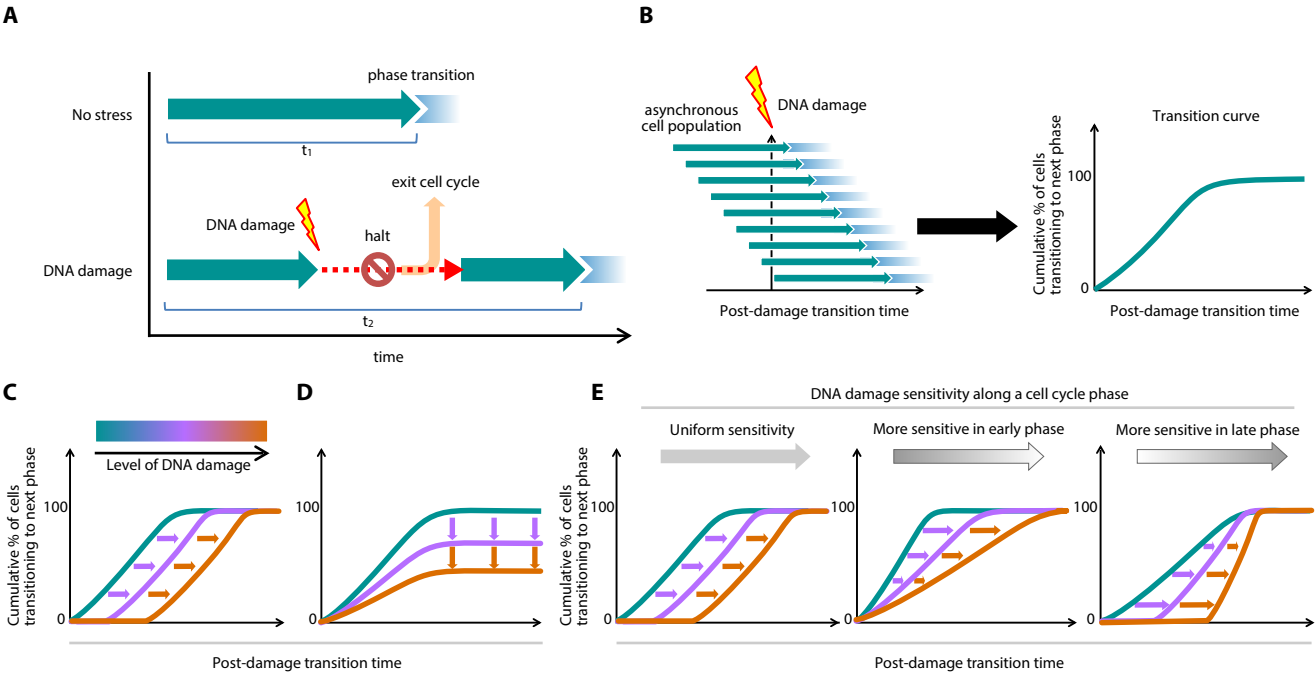
A
No stress
phase transition
t1
exit cell cycle
DNA damage
halt
DNA damage
t2
time
B
asynchronous cell population
DNA damage
Post-damage transition time
Transition curve
Cumulative % of cells transitioning to next phase
100
0
Post-damage transition time
C
Level of DNA damage
Cumulative % of cells transitioning to next phase
100
0
Post-damage transition time
D
100
0
E
DNA damage sensitivity along a cell cycle phase
Uniform sensitivity
More sensitive in early phase
More sensitive in late phase
Cumulative % of cells transitioning to next phase
100
0
Post-damage transition time

Figure 1

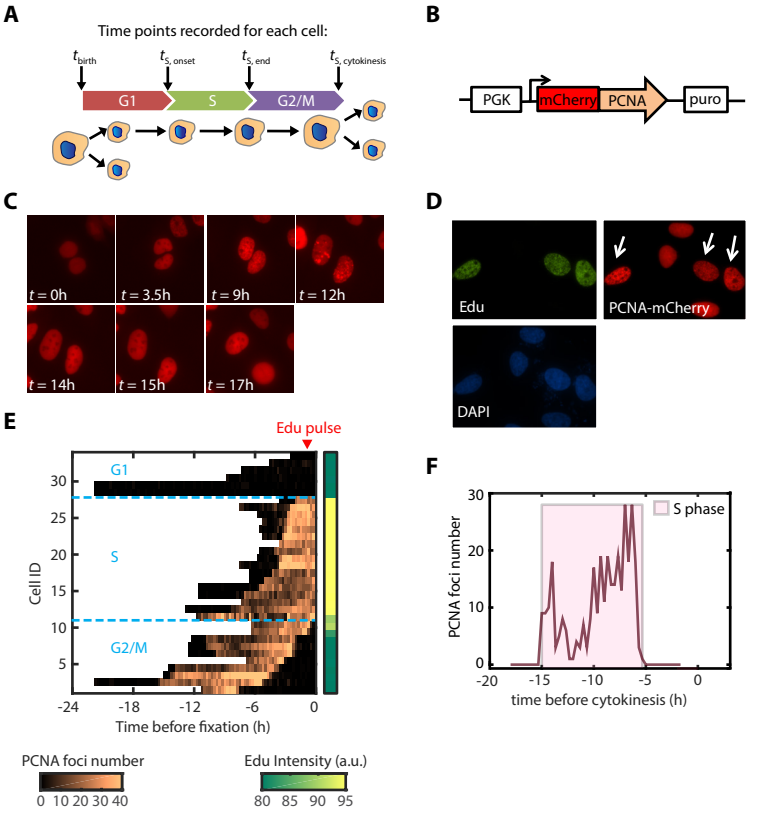
A
Time points recorded for each cell:
t_{birth}
$t_{S, onset}$
$t_{S, end}$
$t_{S, cytokinesis}$
G1
S
G2/M
B
PGK
mCherry
PCNA
puro
C
t = 0h
t = 3.5h
t = 9h
t = 12h
t = 14h
t = 15h
t = 17h
D
Edu
PCNA-mCherry
DAPI
E
Edu pulse
G1
S
G2/M
Cell ID
Time before fixation (h)
PCNA foci number
0 10 20 30 40
Edu Intensity (a.u.)
80 85 90 95
F
S phase
PCNA foci number
time before cytokinesis (h)

Figure 2

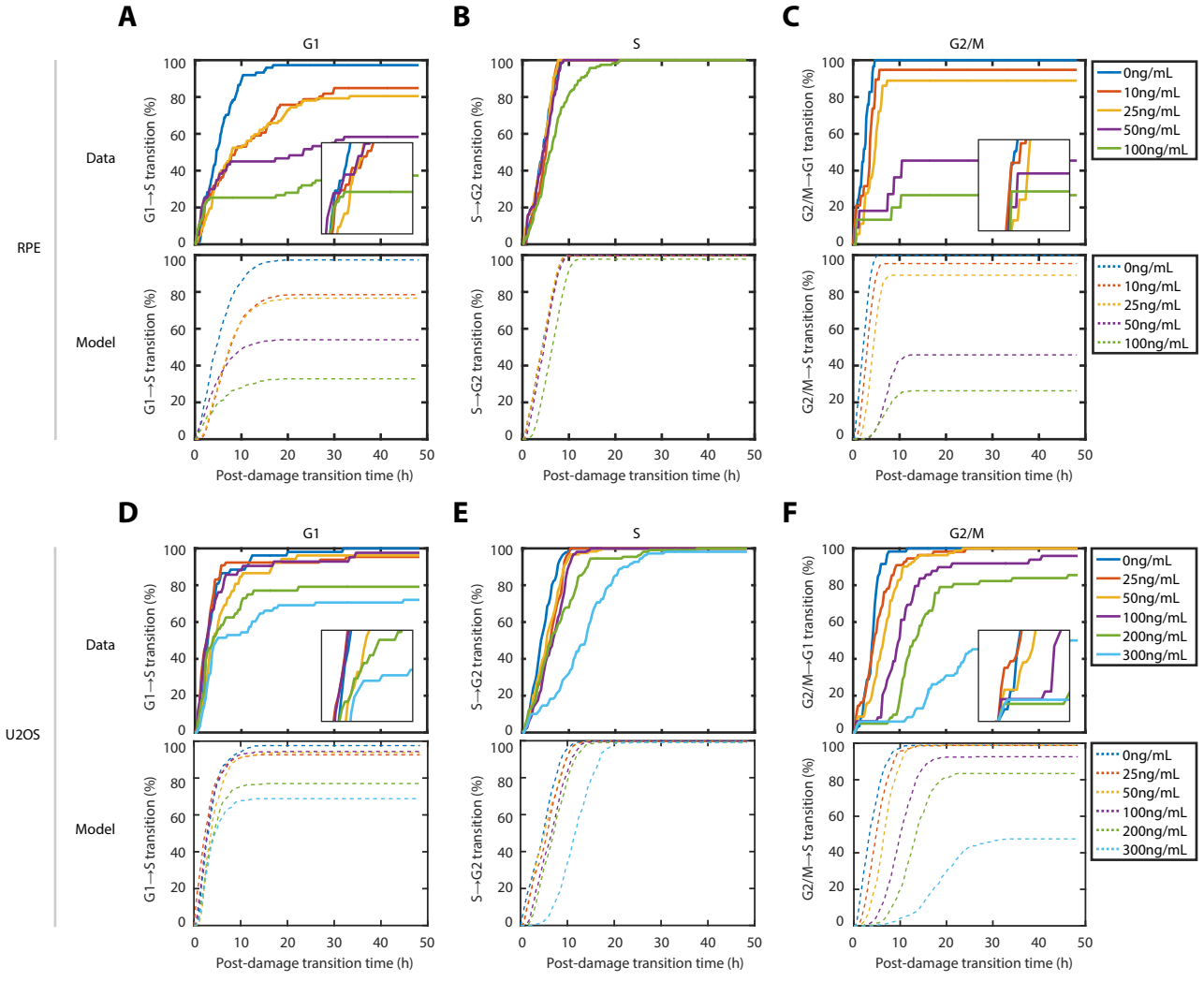
A
B
C
D
E
F
G1
S
G2/M
RPE
U2OS
Data
Model
G1→S transition (%)
S→G2 transition (%)
G2/M→G1 transition (%)
G2/M→S transition (%)
Post-damage transition time (h)
0ng/mL
10ng/mL
25ng/mL
50ng/mL
100ng/mL
200ng/mL
300ng/mL

Figure 3

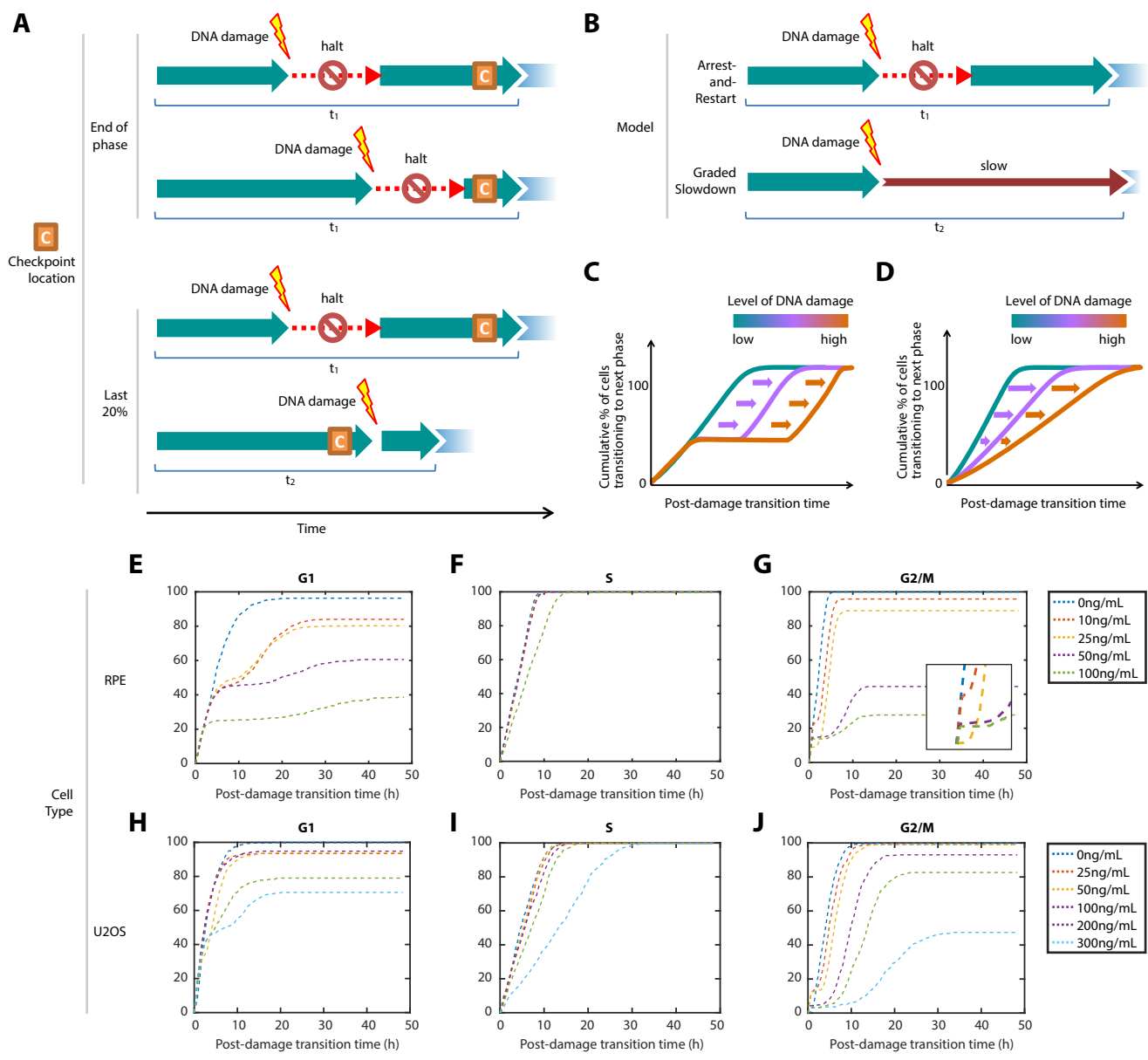
A
DNA damage
halt
C
t1
End of phase
DNA damage
halt
C
t1
C
Checkpoint location
DNA damage
halt
C
t1
Last 20%
DNA damage
C
t2
Time
B
DNA damage
halt
Arrest-and-Restart
t1
Model
DNA damage
slow
Graded Slowdown
t2
C
Level of DNA damage
low
high
Cumulative % of cells transitioning to next phase
100
0
Post-damage transition time
D
Level of DNA damage
low
high
Cumulative % of cells transitioning to next phase
100
0
Post-damage transition time
E
G1
F
S
G
G2/M
RPE
Cell Type
U2OS
H
G1
I
S
J
G2/M
Post-damage transition time (h)
0ng/mL
10ng/mL
25ng/mL
50ng/mL
100ng/mL
0ng/mL
25ng/mL
50ng/mL
100ng/mL
200ng/mL
300ng/mL

Figure 4

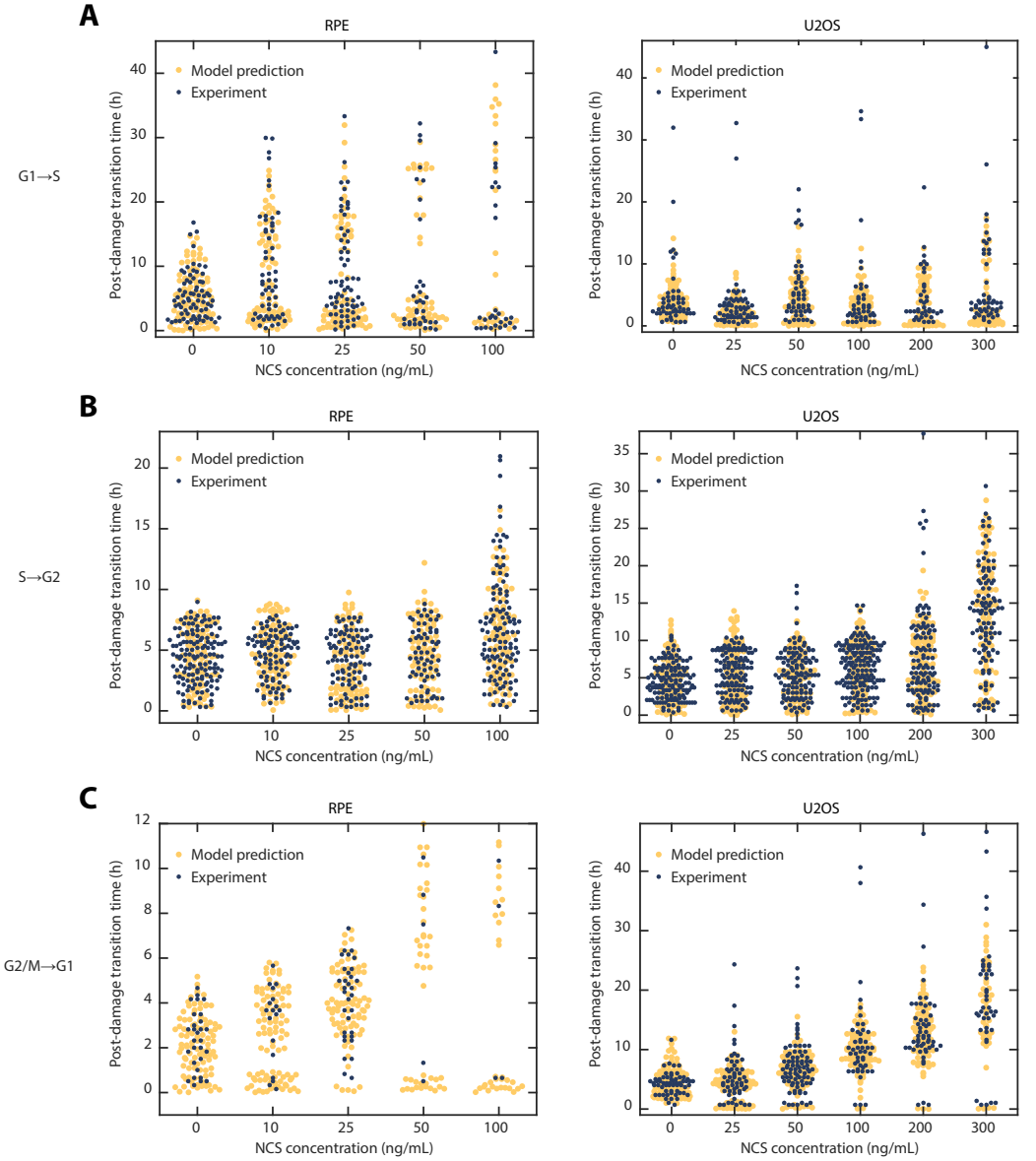
A
RPE
U2OS
G1→S
Model prediction
Experiment
Post-damage transition time (h)
NCS concentration (ng/mL)
B
S→G2
C
G2/M→G1

Figure 5

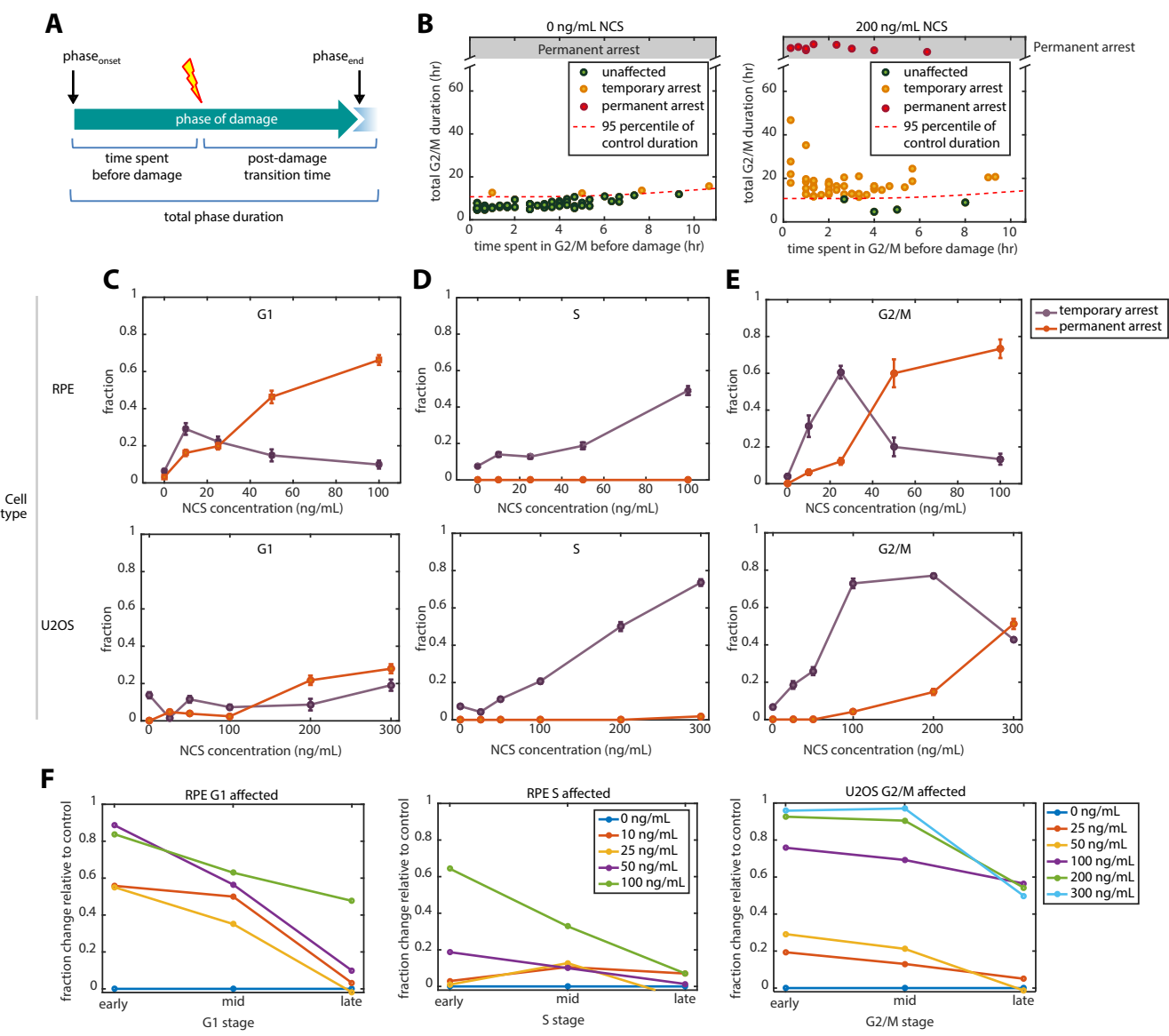
A
phase$_{onset}$
phase$_{end}$
phase of damage
time spent before damage
post-damage transition time
total phase duration
B
0 ng/mL NCS
200 ng/mL NCS
Permanent arrest
unaffected
temporary arrest
permanent arrest
95 percentile of control duration
total G2/M duration (hr)
time spent in G2/M before damage (hr)
C
D
E
G1
S
G2/M
temporary arrest
permanent arrest
Cell type
RPE
U2OS
fraction
NCS concentration (ng/mL)
F
RPE G1 affected
RPE S affected
U2OS G2/M affected
0 ng/mL
10 ng/mL
25 ng/mL
50 ng/mL
100 ng/mL
200 ng/mL
300 ng/mL
fraction change relative to control
early
mid
late
G1 stage
S stage
G2/M stage

Figure 6

	G1	S	G2
Checkpoint location			
Checkpoint kinetics	Severe damage: all-or-none Mild damage: continuous slowdown	Continuous slowdown	All-or-none
Halt duration	Fixed at high concentration	Not present	Increases with damage level
Sensitivity	Sensitive	Insensitive	Most sensitive
Cell cycle outcome	Predominantly permanent arrest	Always temporary arrest	Drastic switch from temporary to permanent arrest

Table 1

bioRxiv preprint doi: https://doi.org/10.1101/137307; this version posted May 12, 2017. The copyright holder for this preprint (which was not certified by peer review) is the author/funder, who has granted bioRxiv a license to display the preprint in perpetuity. It is made available under aCC-BY 4.0 International license.

Supplementary Material for:

DNA damage checkpoint dynamics drive cell cycle phase transitions

Hui Xiao Chao[1,2], Cere E. Poovey[1], Ashley A. Privette[1], Gavin D. Grant[3,4], Jeanette G. Cook[3,4], and Jeremy E. Purvis[1,2,4,†]

[1]Department of Genetics
[2]Curriculum for Bioinformatics and Computational Biology
[3]Department of Biochemistry and Biophysics
[4]Lineberger Comprehensive Cancer Center

University of North Carolina, Chapel Hill
120 Mason Farm Road
Chapel Hill, NC 27599-7264

[†]Corresponding Author:
Jeremy Purvis
Genetic Medicine Building 5061, CB#7264
120 Mason Farm Road
Chapel Hill, NC 27599-7264
jeremy_purvis@med.unc.edu

bioRxiv preprint doi: https://doi.org/10.1101/137307; this version posted May 12, 2017. The copyright holder for this preprint (which was not certified by peer review) is the author/funder, who has granted bioRxiv a license to display the preprint in perpetuity. It is made available under aCC-BY 4.0 International license.

Model simulations and parameter fitting

All simulations and parameter fitting were performed using MATLAB. The durations of each cell cycle phase—G1, S, or G2/M—under basal conditions were fitted to an Erlang distribution (**Figure S5**). The Erlang distribution was chosen for three reasons. First, it contains two independent parameters, the minimal number of parameters needed to describe distributions of varying mean and variance. Second, the Erlang distribution has a simple and relevant biological interpretation: each cell cycle phase can be viewed as a multistep biochemical process that needs to be completed sequentially in order to advance to the next cell cycle phase. Alternatively, the multistep process can be viewed as the accumulation of a clock protein whose number needs to exceed a certain threshold value before transitioning to the next cell cycle phase [1]. Third, the Erlang distribution provides an appropriate framework to carry out stochastic simulations that are biologically interpretable. This framework is also flexible to modifications of the checkpoint dynamics, such as implementing an all-or-none or graded slowdown, as well as introducing a temporally located commitment point within a particular cell cycle phase.

By fitting the experimental distribution of cell cycle phase durations, we obtained two parameters: shape—which can be interpreted as the number of steps within a cell cycle phase—and scale—which can be interpreted as the average timescale for each of the steps. Using the estimated parameters, we then simulated the cell cycle phase transitions in an asynchronous population with phase durations drawn from the distribution under basal conditions.

Fitting with the “arrest-and-restart” checkpoint model

Under the arrest-and-restart checkpoint model, the checkpoint implements a complete halt and a permanent arrest probability. Therefore, we incorporated these two properties by introducing two free parameters: delay duration, which was drawn from a normal distribution with standard deviation proportional to the mean, and a permanent arrest probability, into our simulations. We then estimated the parameters using the fminsearch function in MATLAB to minimize the mean square difference between the simulation and experimental data.

Fitting with the refined checkpoint model

In addition to delay duration and permanent arrest probability, as in the arrest-and-restart checkpoint model, we introduced a free parameter—commitment point—to allow for checkpoint escape once the cell cycle phase progression passes that temporally located commitment point. In addition to the above framework that described an all-or-none kinetics, we also performed simulation under the graded slowdown kinetic by allowing the scale parameter (from the fitted Erlang distribution), which related to the rate of progression under basal conditions, to change.

1. Ghusinga, K. R. *et al.* A mechanistic stochastic framework for regulating bacterial cell division. *Sci. Rep.* **6,** 30229 (2016).

bioRxiv preprint doi: https://doi.org/10.1101/137307; this version posted May 12, 2017. The copyright holder for this preprint (which was not certified by peer review) is the author/funder, who has granted bioRxiv a license to display the preprint in perpetuity. It is made available under aCC-BY 4.0 International license.

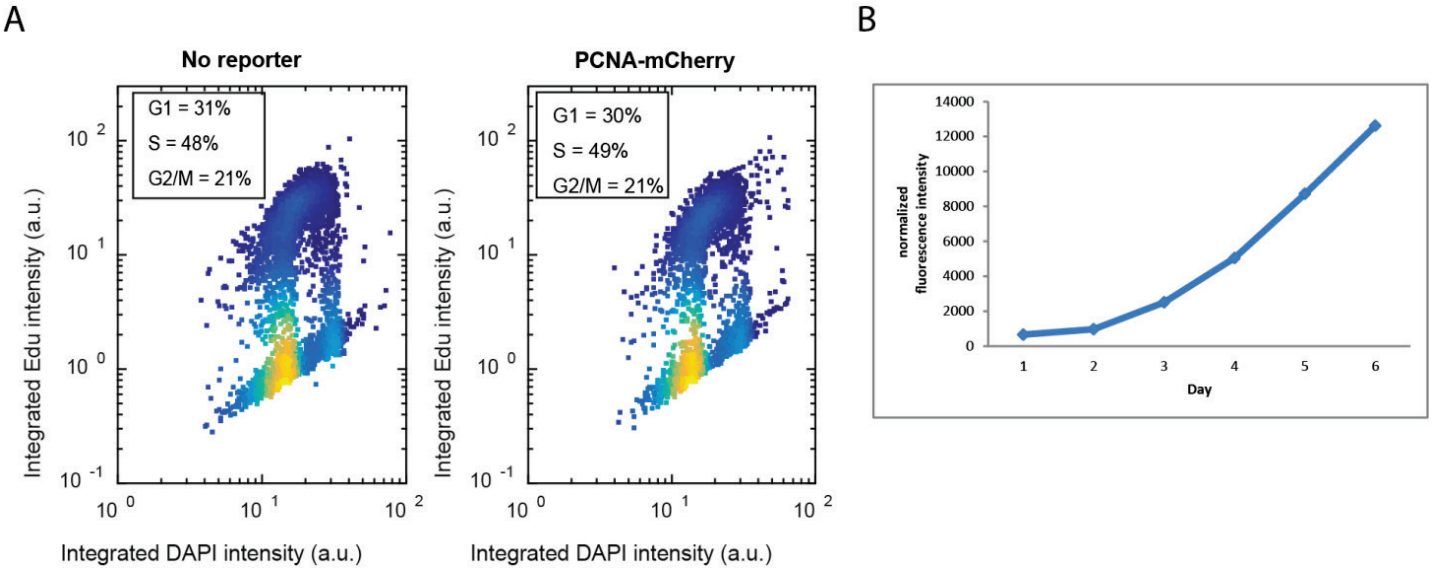

Figure S1. Cell cycle progression is not disturbed by the live cell reporters.

A. Cell cycle distribution of U2OS cells. Cells with (left panel) and without (right panel) expressing PCNA-mCherry were pulsed with 10 μM EdU for 1 hour, followed by fixation, staining, and quantification for EdU incorporation and DAPI content.

B. The doubling time of the cell line in culture was consistent with the cell cycle durations measured from live-cell image. The doubling time (20.1 hours) was measured by fitting the most rapid phase of the growth curve with an exponential function. Relative cell count was quantified using the CellTiter blue assay using U2OS cells.

bioRxiv preprint doi: https://doi.org/10.1101/137307; this version posted May 12, 2017. The copyright holder for this preprint (which was not certified by peer review) is the author/funder, who has granted bioRxiv a license to display the preprint in perpetuity. It is made available under aCC-BY 4.0 International license.

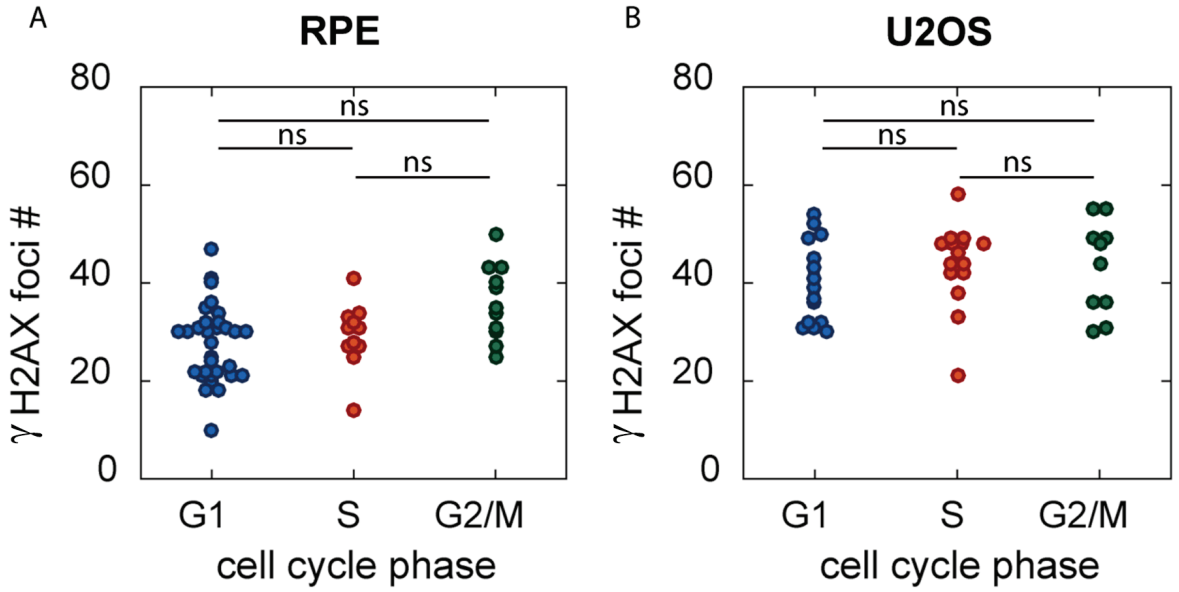

Figure S2. The amounts of DSBs induced by NCS were similar in each cell cycle phase.

(A) RPE and (B) U2OS cells were induced with 100 ng/mL and 300 ng/mL NCS, respectively, for 30 minutes, and pulsed with 10 μM EdU for 15 minutes before fixation. The cells were then stained for γH2AX and DAPI to quantify the level of DSBs and DNA content, respectively. The cell cycle phase was designated based on the EdU and DAPI intensity. ns indicates not significant based on significance level of p=0.05 based on Kolmogorov–Smirnov test.

bioRxiv preprint doi: https://doi.org/10.1101/137307; this version posted May 12, 2017. The copyright holder for this preprint (which was not certified by peer review) is the author/funder, who has granted bioRxiv a license to display the preprint in perpetuity. It is made available under aCC-BY 4.0 International license.

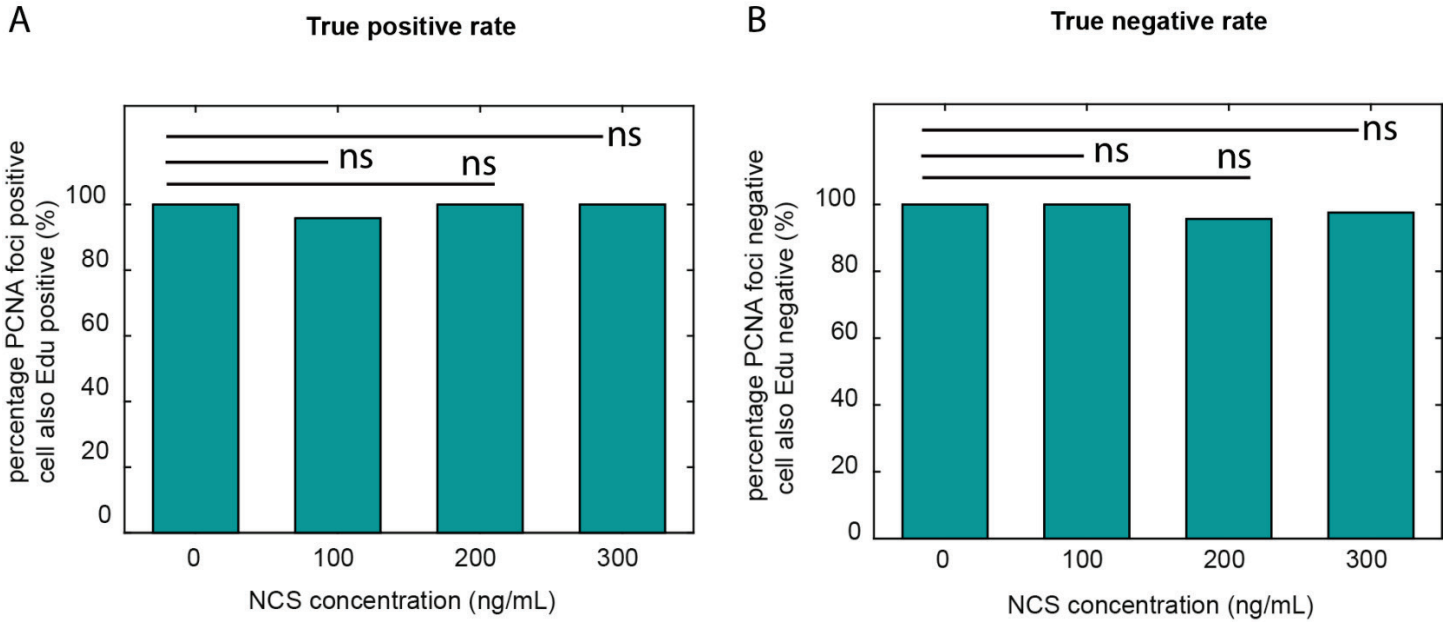

Figure S3. The PCNA-mCherry is a good S phase reporter under induced DNA damage by NCS.

A-B. The true positive rate (A) and true negative rate (B) of the PCNA foci as a marker for S phase, measured by EdU incorporation. U2OS cells were treated with NCS of indicated concentrations under live-cell imaging conditions to quantify for PCNA foci. 10 hrs after the treatment, cells were pulsed with 10 μM EdU for 20 mins, followed by fixation, staining, and scoring for EdU incorporation. ns indicates not significant based on significance level of p=0.05 based on Fisher's exact test. In addition, we did not observe DNA damage-induced PCNA foci in G1 or G2 under our conditions, which could cause the cells to be erroneously scored as having entered S phase.

bioRxiv preprint doi: https://doi.org/10.1101/137307; this version posted May 12, 2017. The copyright holder for this preprint (which was not certified by peer review) is the author/funder, who has granted bioRxiv a license to display the preprint in perpetuity. It is made available under aCC-BY 4.0 International license.

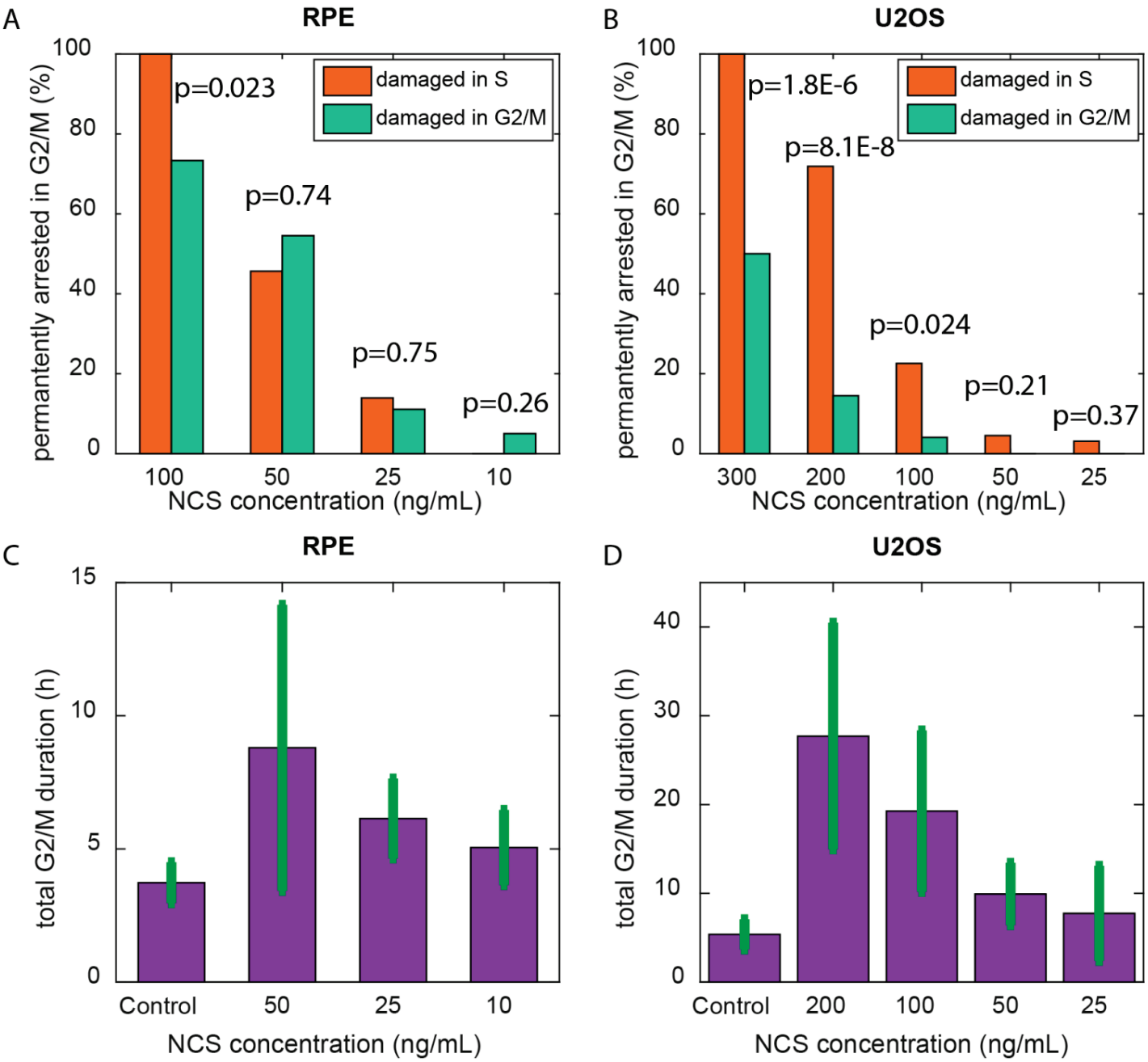

Figure S4. Cells damaged in S phase were arrested in the subsequent G2 phase.

A-B. RPE (A) and U2OS (B) cells that were damaged in S and G2/M were quantified for the fractions of being rested in G2/M arrest by the end of 48hr hour post damage. The p-values were calculated based on the Fisher's exact test.

C-D. RPE (C) and U2OS (D) cells that were damaged in S and completed the subsequent G2/M were quantified for the G2/M durations. Control represents cells without NCS treatment. Error bars represent standard deviations.

bioRxiv preprint doi: https://doi.org/10.1101/137307; this version posted May 12, 2017. The copyright holder for this preprint (which was not certified by peer review) is the author/funder, who has granted bioRxiv a license to display the preprint in perpetuity. It is made available under aCC-BY 4.0 International license.

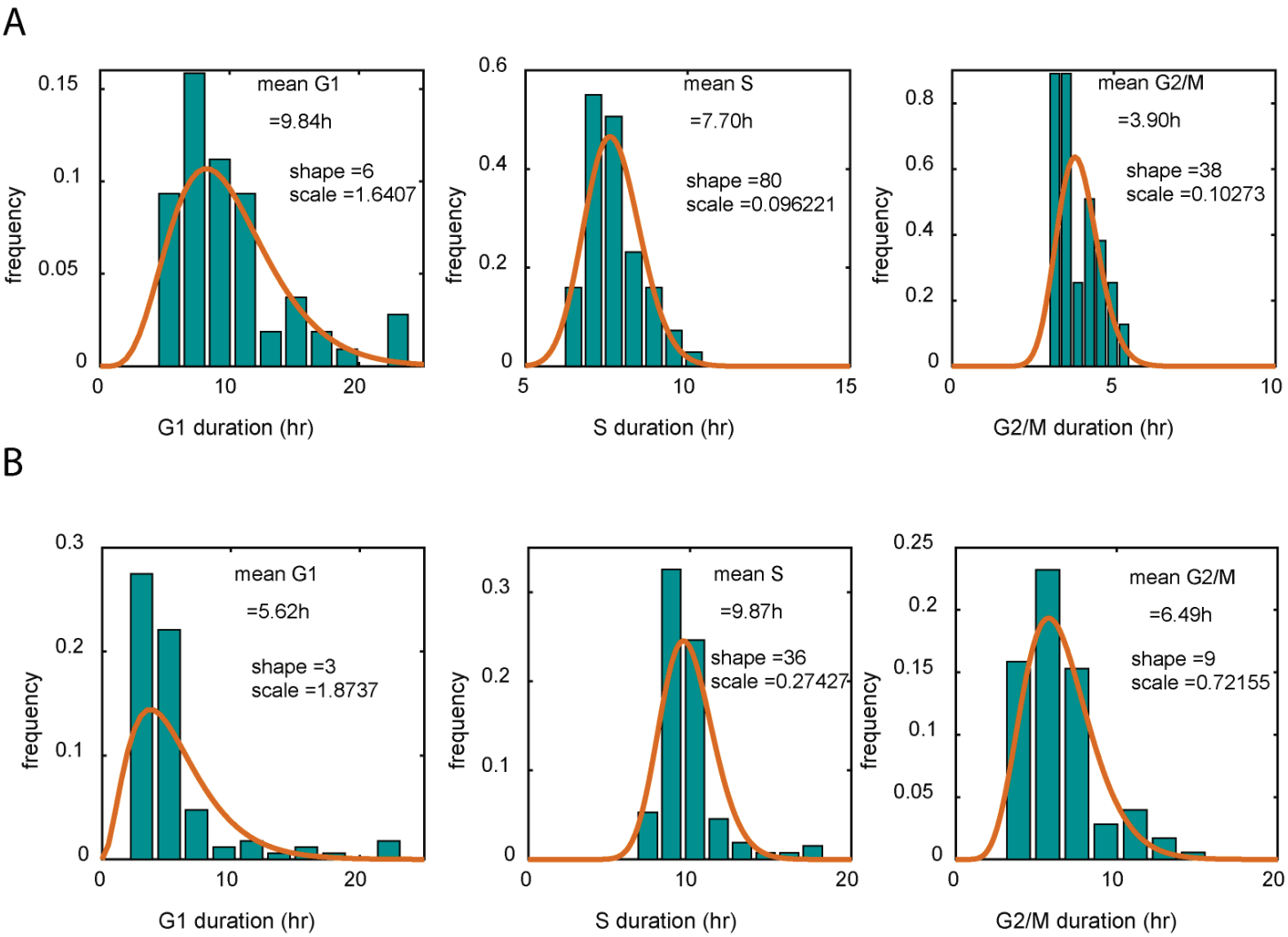

Figure S5. Cell cycle phase distribution fitted with Erlang distribution.

A-B. Asynchronously proliferating RPE (A) and U2OS (B) cells were quantified for their cell cycle phase (G1, S, G2/M) durations based PCNA-mCherry morphology using time-lapse microscopy. The distribution of the cell cycle phase were fitted with Erlang distribution to estimate the shape and scale parameters.

bioRxiv preprint doi: https://doi.org/10.1101/137307; this version posted May 12, 2017. The copyright holder for this preprint (which was not certified by peer review) is the author/funder, who has granted bioRxiv a license to display the preprint in perpetuity. It is made available under aCC-BY 4.0 International license.

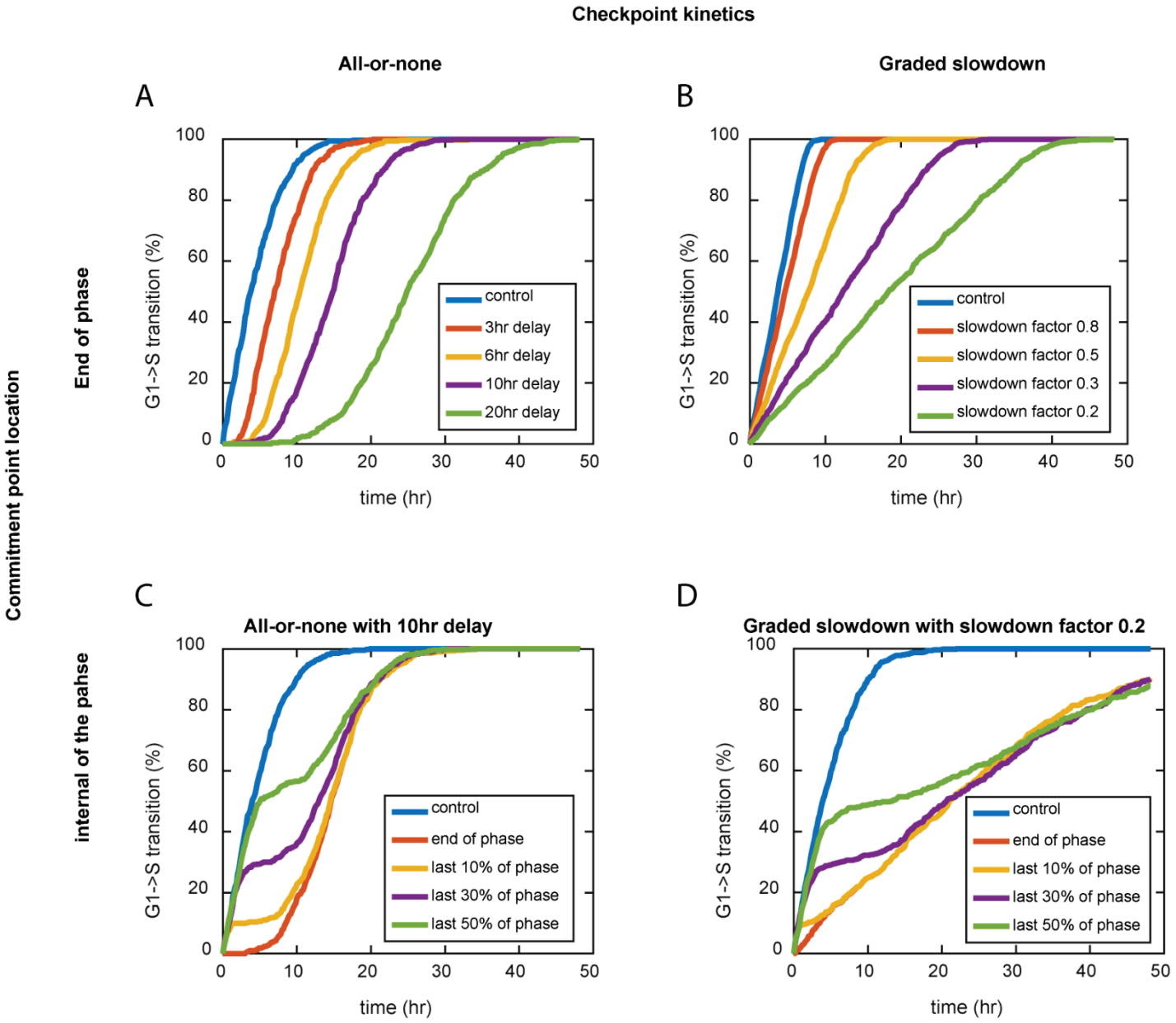

Figure S6. Each cell cycle phase implements a distinct DNA damage checkpoint dynamics.

A-B. Simulation of cell cycle transition dynamics upon DNA damage under the (A) all-or-none kinetics with varying halt duration, or (B) graded slowdown kinetics with varying slowdown factor.

C-D. Simulation of cell cycle transition dynamics as A and B, but incorporated the commitment point of varying location.

bioRxiv preprint doi: https://doi.org/10.1101/137307; this version posted May 12, 2017. The copyright holder for this preprint (which was not certified by peer review) is the author/funder, who has granted bioRxiv a license to display the preprint in perpetuity. It is made available under aCC-BY 4.0 International license.

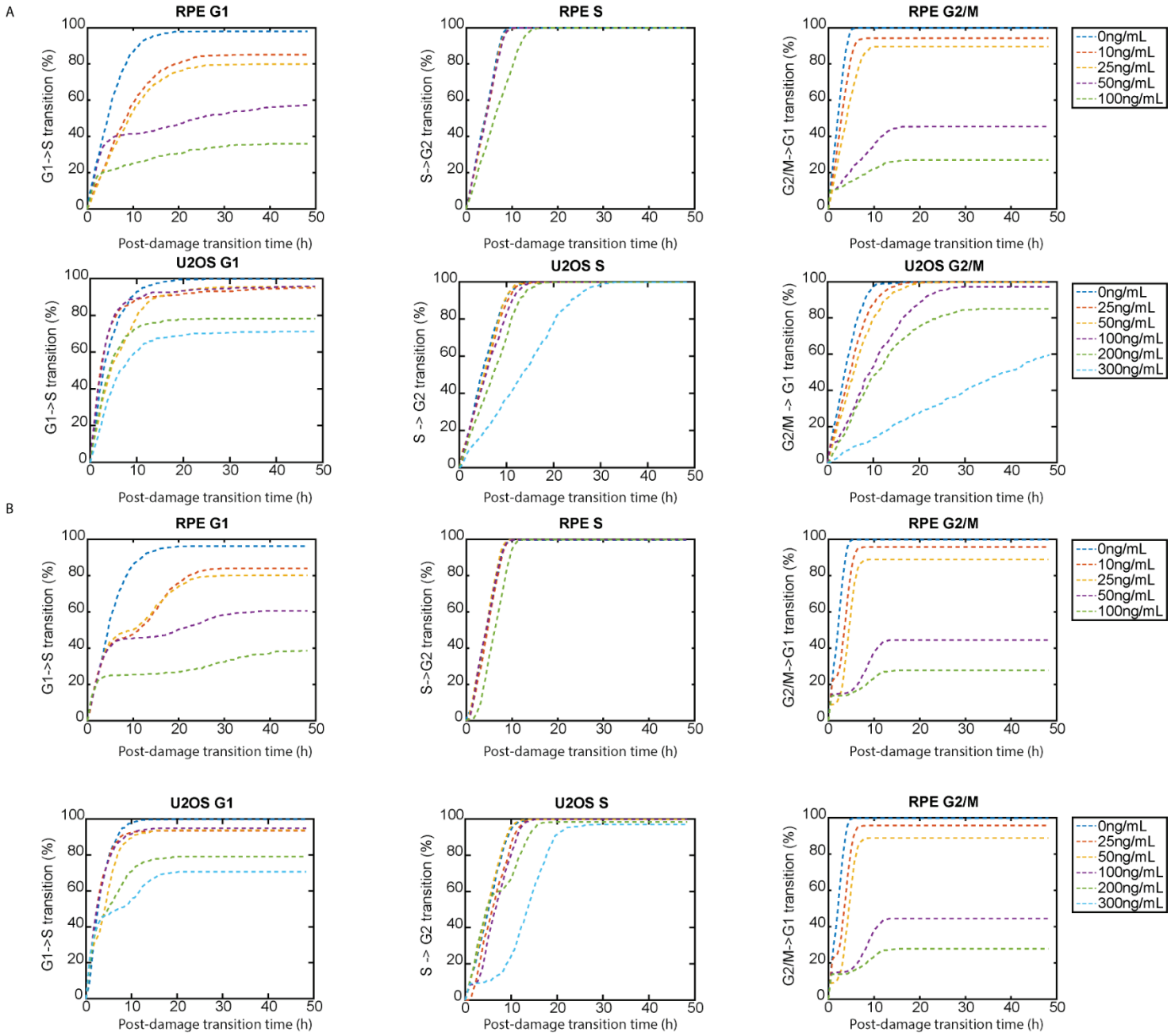

Figure S7. Model fitting of cell cycle phase-specific transition curves in response to acute DNA damage, as in lower panels of Figure 3, but fitted with the refined model that incorporated both the flexible commitment point location and the possibility of graded slowdown checkpoint kinetics. Each condition was fitted with the (A) graded slowdown or (B) all-or-none checkpoint kinetics.

bioRxiv preprint doi: https://doi.org/10.1101/137307; this version posted May 12, 2017. The copyright holder for this preprint (which was not certified by peer review) is the author/funder, who has granted bioRxiv a license to display the preprint in perpetuity. It is made available under aCC-BY 4.0 International license.

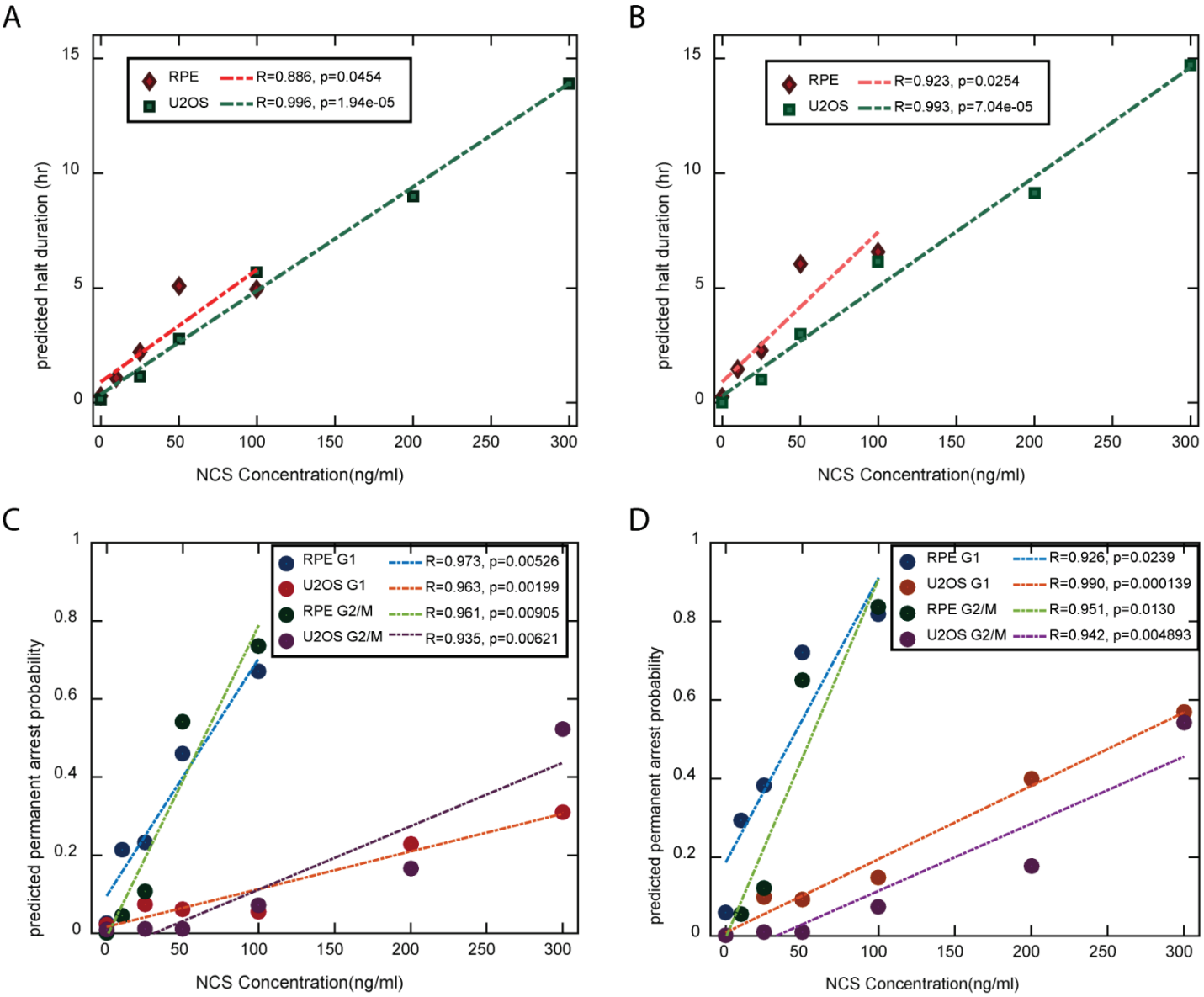

Figure S8. Model estimations of the checkpoint halt duration and permanent arrest probability as a function of DNA damage level.

A. By fitting the data with the “arrest-and-restart” model, we estimated the halt durations in G2/M in response to the indicated NCS concentrations.

B. Same as A, but the data were fitted with the refined model with a flexible commitment point.

C. By fitting the data with the “arrest-and-restart” model, we estimated the permanent arrest probabilities in G1 and G2/M in response to the indicated NCS concentrations.

D. Same as C, but the data were fitted with the refined model with a flexible commitment point.

bioRxiv preprint doi: https://doi.org/10.1101/137307; this version posted May 12, 2017. The copyright holder for this preprint (which was not certified by peer review) is the author/funder, who has granted bioRxiv a license to display the preprint in perpetuity. It is made available under aCC-BY 4.0 International license.

A

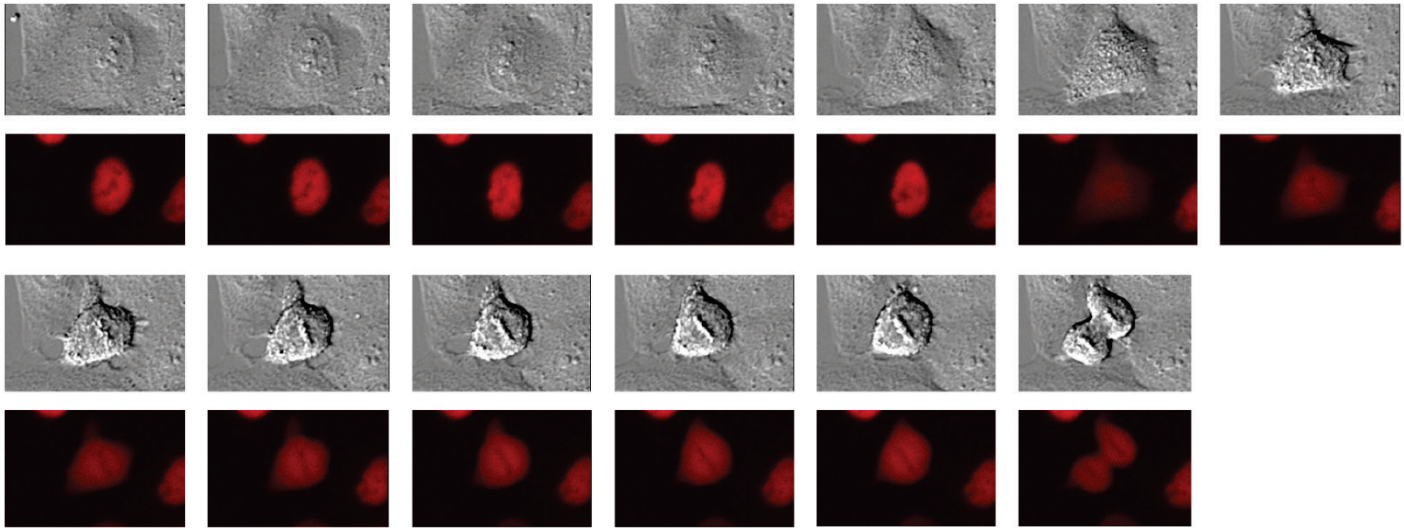

B

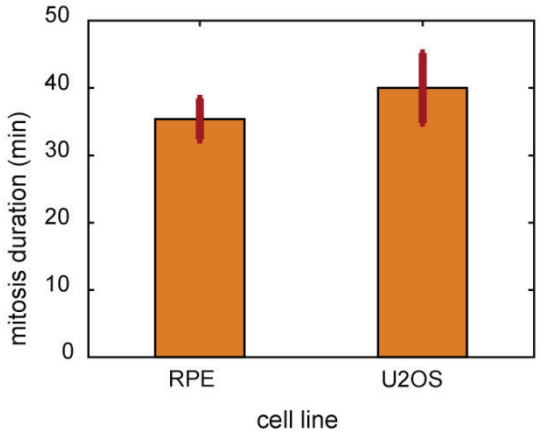

Figure S9. Mitosis durations in RPE and U2OS.

A. Live-cell images of U2OS undergoing mitosis. Upper row: differential interference contrast (DIC). Lower row: mCherry channel.

B. Mitosis durations based on nuclear envelope breakdown revealed by both the DIC and mCherry channels. Error bars represent standard error of mean (n=10).

bioRxiv preprint doi: https://doi.org/10.1101/137307; this version posted May 12, 2017. The copyright holder for this preprint (which was not certified by peer review) is the author/funder, who has granted bioRxiv a license to display the preprint in perpetuity. It is made available under aCC-BY 4.0 International license.

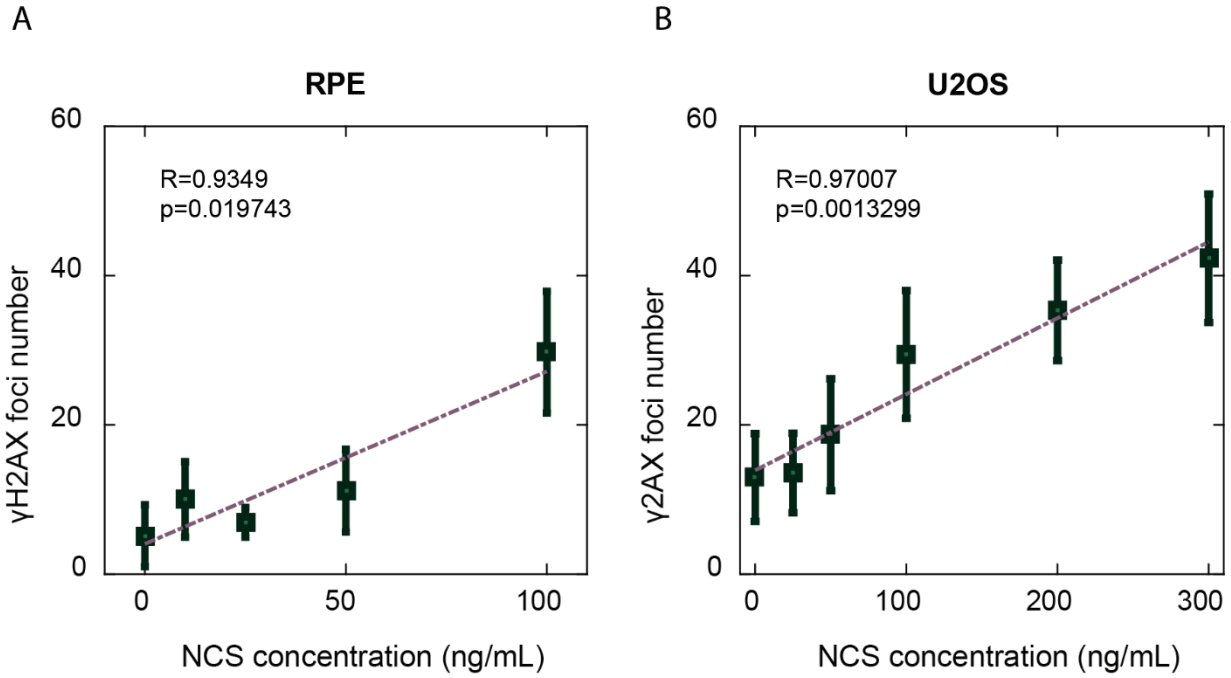

Figure S10. Linear relationship between NCS concentrations and γH2AX foci number in (A) RPE and (B) U2OS cells. Asynchronous cells were treated with NCS of indicated concentrations, and after 60 minutes, cells were fixed, stained, and quantified for their γH2AX foci numbers. The data were fitted the linear regression. Error bars represent standard error of mean.

bioRxiv preprint doi: https://doi.org/10.1101/137307; this version posted May 12, 2017. The copyright holder for this preprint (which was not certified by peer review) is the author/funder, who has granted bioRxiv a license to display the preprint in perpetuity. It is made available under aCC-BY 4.0 International license.

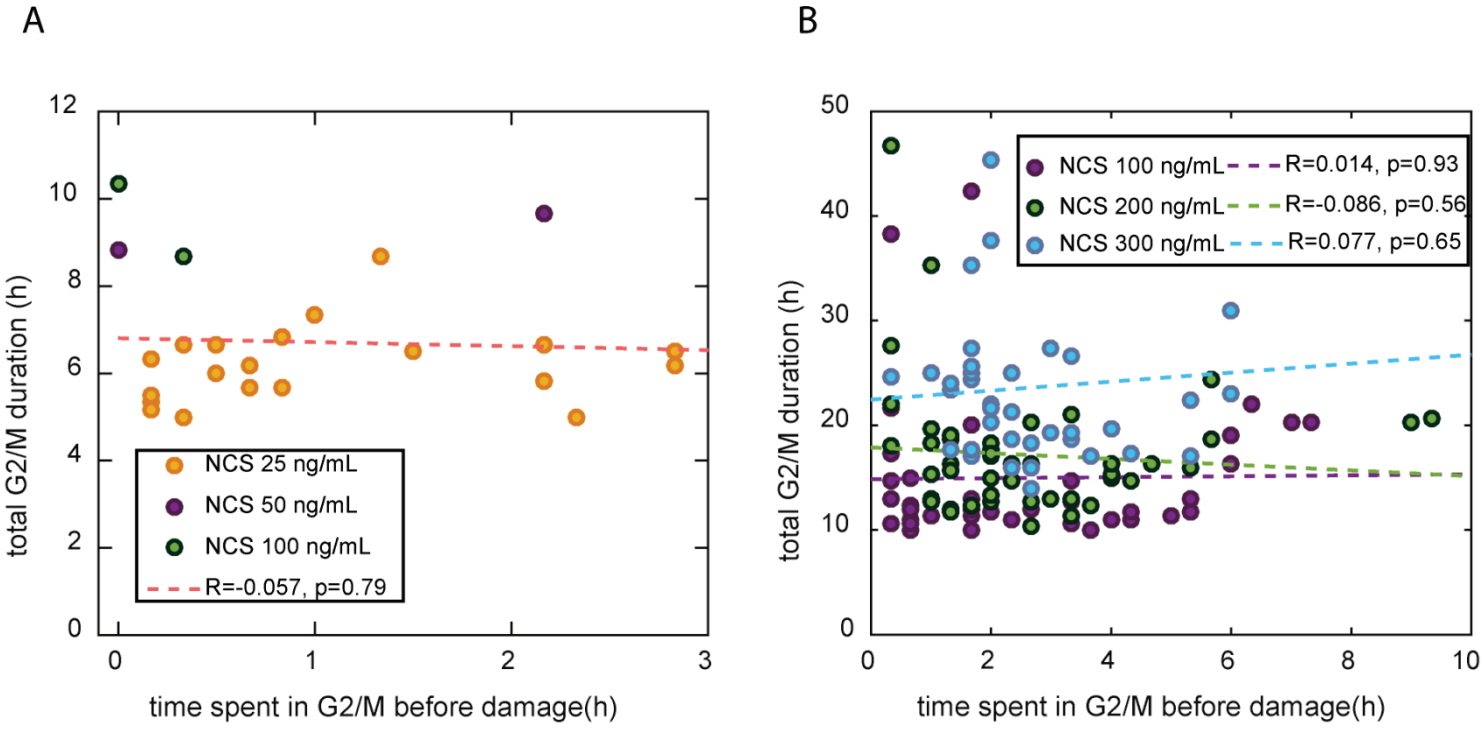

Figure S11. The halt durations imposed in G2/M were independent of the timing of DNA damage throughout the cell cycle phase. (A) RPE and (B) U2OS cells were treated with the indicated NCS concentrations and followed for phase transitions. The total G2/M durations were plotted against the time spent in G2/M before damage. The data were fitted with linear regression.

bioRxiv preprint doi: https://doi.org/10.1101/137307; this version posted May 12, 2017. The copyright holder for this preprint (which was not certified by peer review) is the author/funder, who has granted bioRxiv a license to display the preprint in perpetuity. It is made available under aCC-BY 4.0 International license.

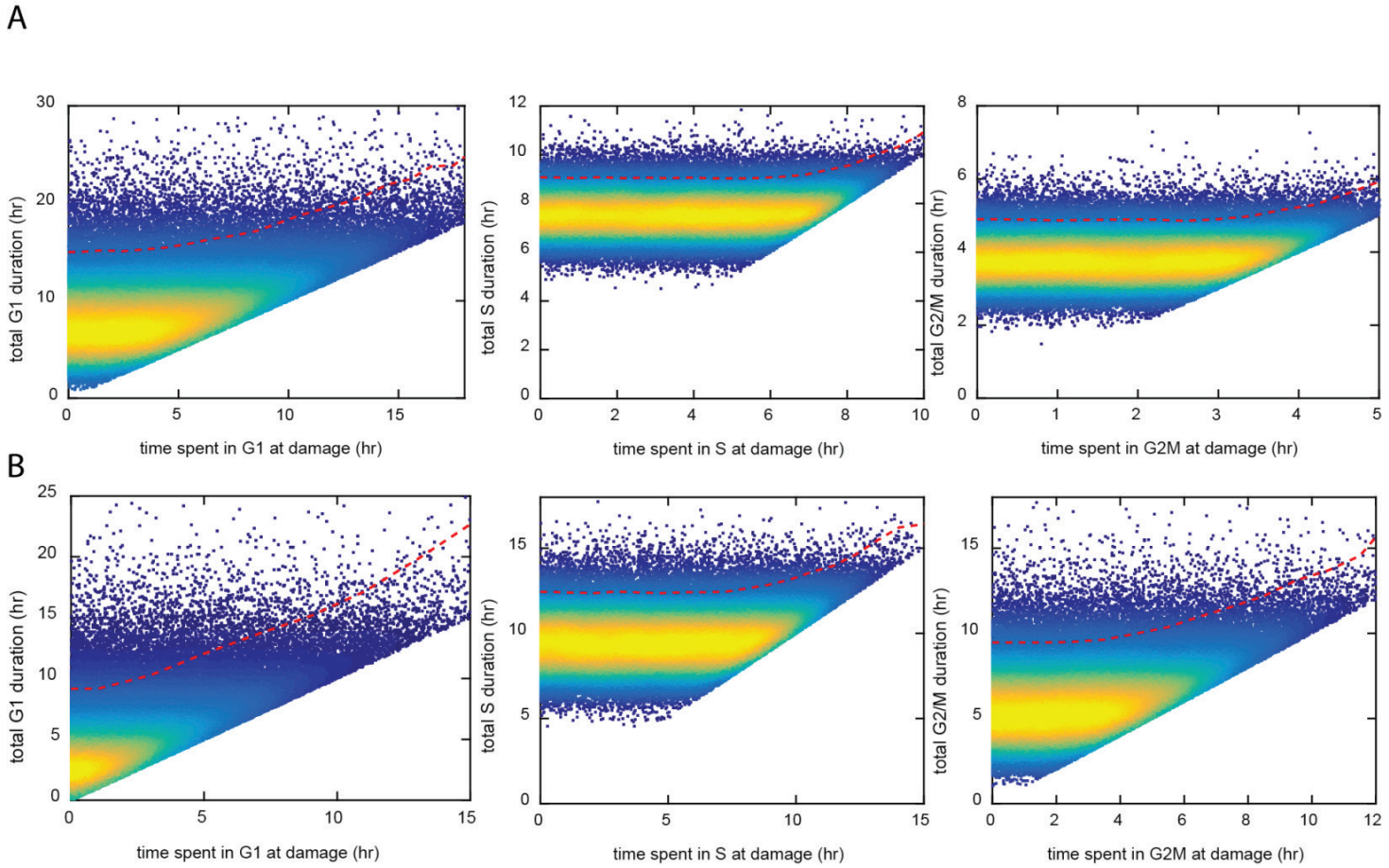

Figure S12. Simulation of cell cycle phase duration produced the 95 percentile cell cycle duration from simulation. Simulation parameters were obtained from the control's cell cycle phase durations of (A) RPE and (B) U2OS, fitted with Erlang distribution. Each point represents a single simulated cell, with color representing the density (heat map). The red dashed lines represent the 95 percentile of the total S phase duration for a given time spent in that phase at damage.

bioRxiv preprint doi: https://doi.org/10.1101/137307; this version posted May 12, 2017. The copyright holder for this preprint (which was not certified by peer review) is the author/funder, who has granted bioRxiv a license to display the preprint in perpetuity. It is made available under aCC-BY 4.0 International license.

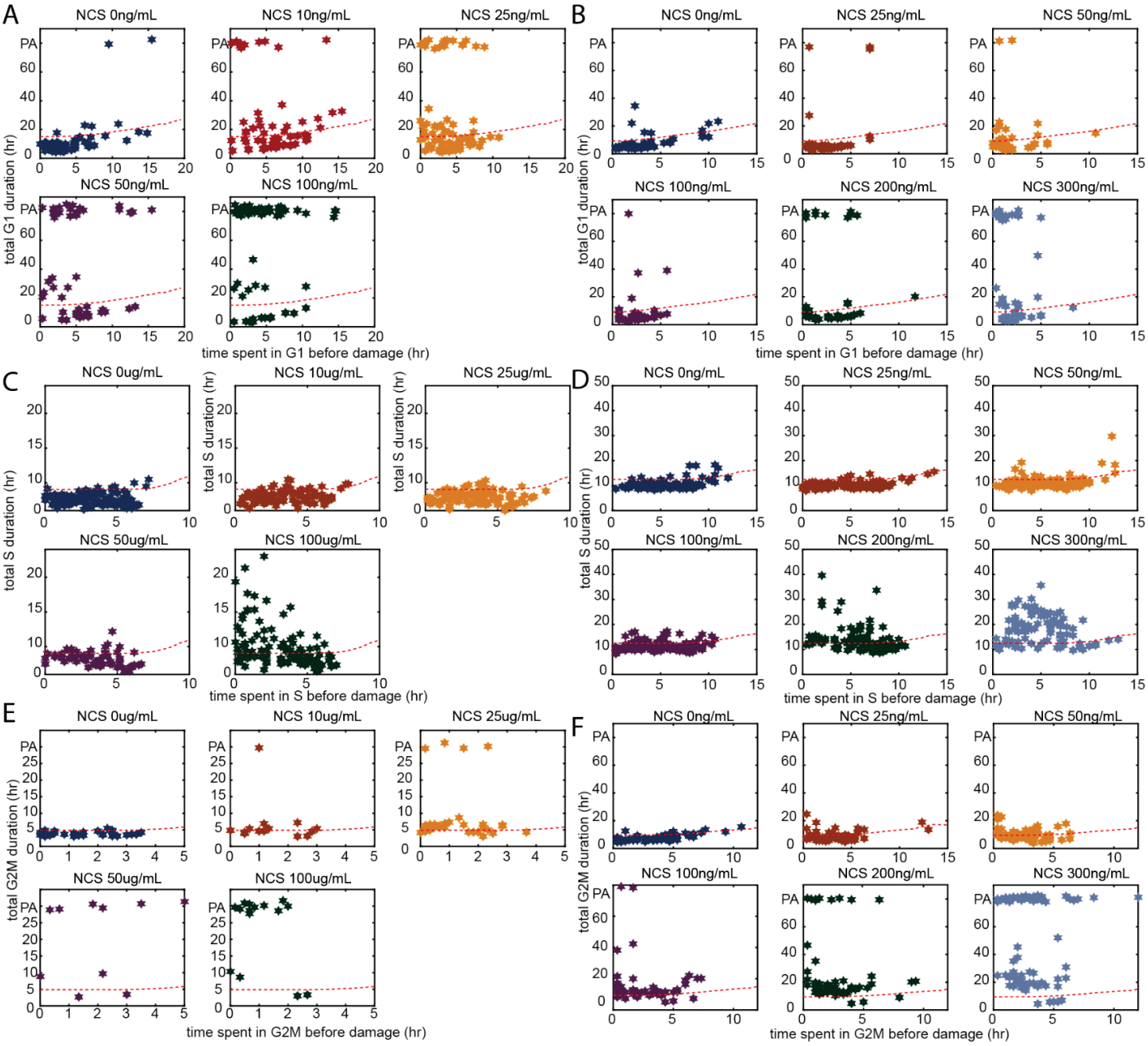

Figure S13. Cell cycle response as a function of cell cycle progress into the phase of damage in (A, C, E) RPE and U2OS (B, D, F). The total cell cycle phase durations were plotted against the time spent in that phase at the time of damage. The 95 percentile lines (red dashed lines) obtained from **Figure S11** were superimposed onto these plots. This analysis allows for designating each single cell into the three outcome categories, as in Figure 6B. PA indicates permanent arrest.

bioRxiv preprint doi: https://doi.org/10.1101/137307; this version posted May 12, 2017. The copyright holder for this preprint (which was not certified by peer review) is the author/funder, who has granted bioRxiv a license to display the preprint in perpetuity. It is made available under aCC-BY 4.0 International license.

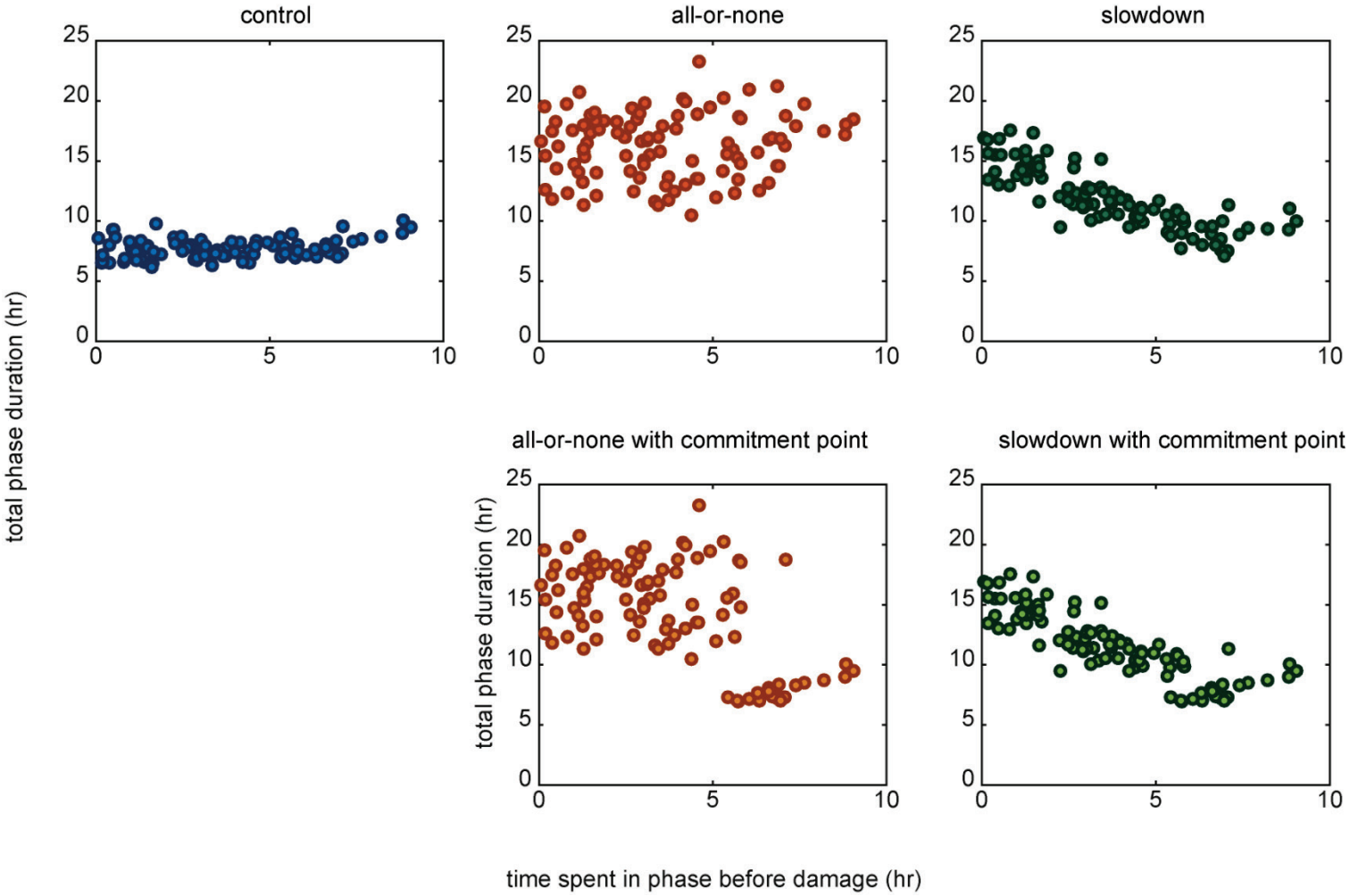

Figure S14. Model simulation demonstrating the timing of DNA damage within cell cycle phase stage affects the total phase duration.

Simulations of cell cycle phase durations as a function of time spent in that phase before damage. Simulations were performed using the fitted parameters from RPE S phase distribution. In the cases with all-or-none checkpoint kinetics, the delay duration was 8 hrs. In the cases with graded slowdown checkpoint kinetics, the slowdown factor was 0.5. In the cases with an internal commitment point, the location was 75% of the entire phase from the onset of the phase.

bioRxiv preprint doi: https://doi.org/10.1101/137307; this version posted May 12, 2017. The copyright holder for this preprint (which was not certified by peer review) is the author/funder, who has granted bioRxiv a license to display the preprint in perpetuity. It is made available under aCC-BY 4.0 International license.

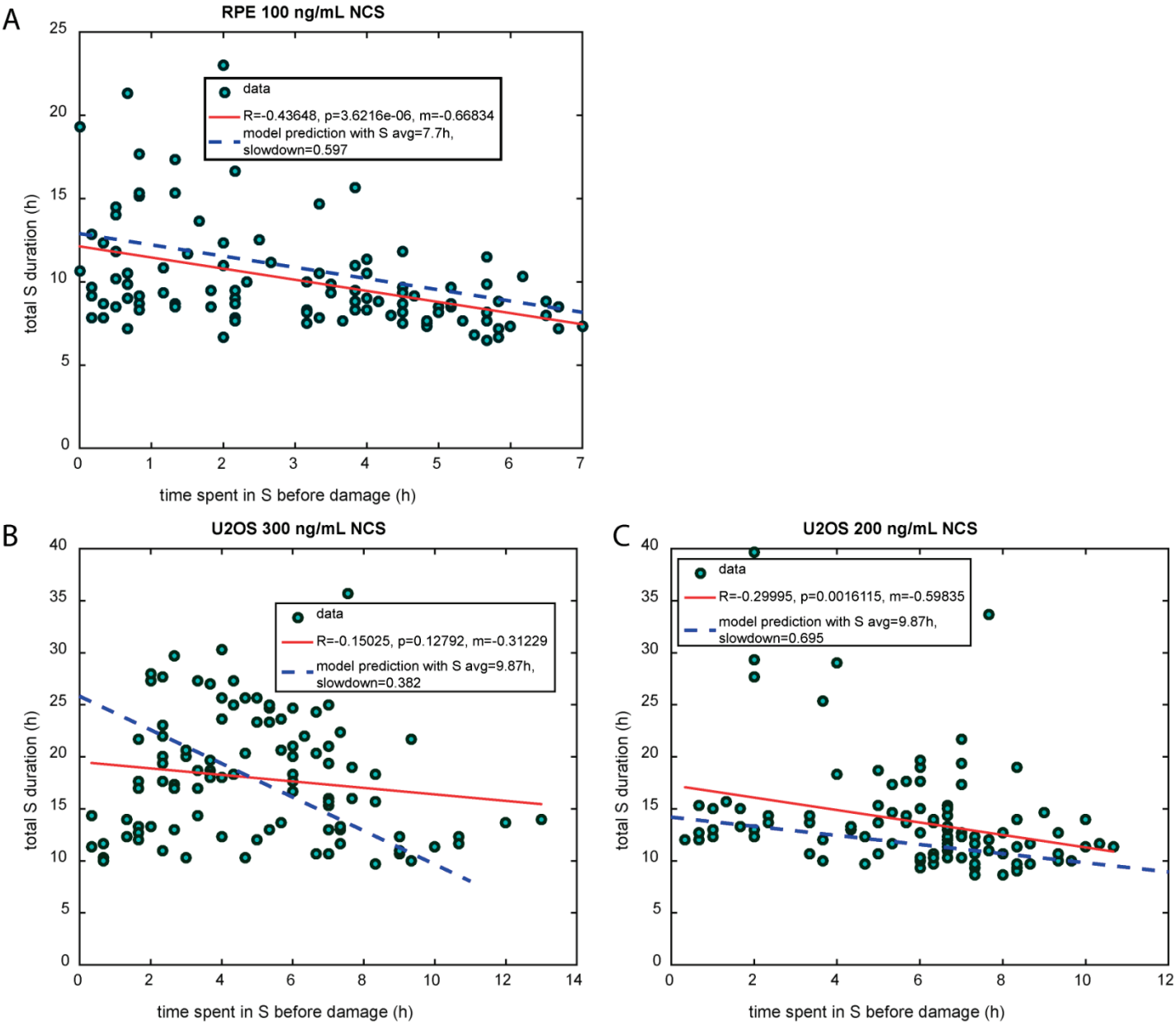

Figure S15. The delay in S phase completion linearly depends on the timing of DNA damage within S phase.

Experimental data of the total S phase durations as a function of time spent in S phase before damage. Red lines represent linear regression of the experimental data. Blue dash lines represent the model predictions of the mean S phase durations based on the graded slowdown checkpoint kinetics.

bioRxiv preprint doi: https://doi.org/10.1101/137307; this version posted May 12, 2017. The copyright holder for this preprint (which was not certified by peer review) is the author/funder, who has granted bioRxiv a license to display the preprint in perpetuity. It is made available under aCC-BY 4.0 International license.

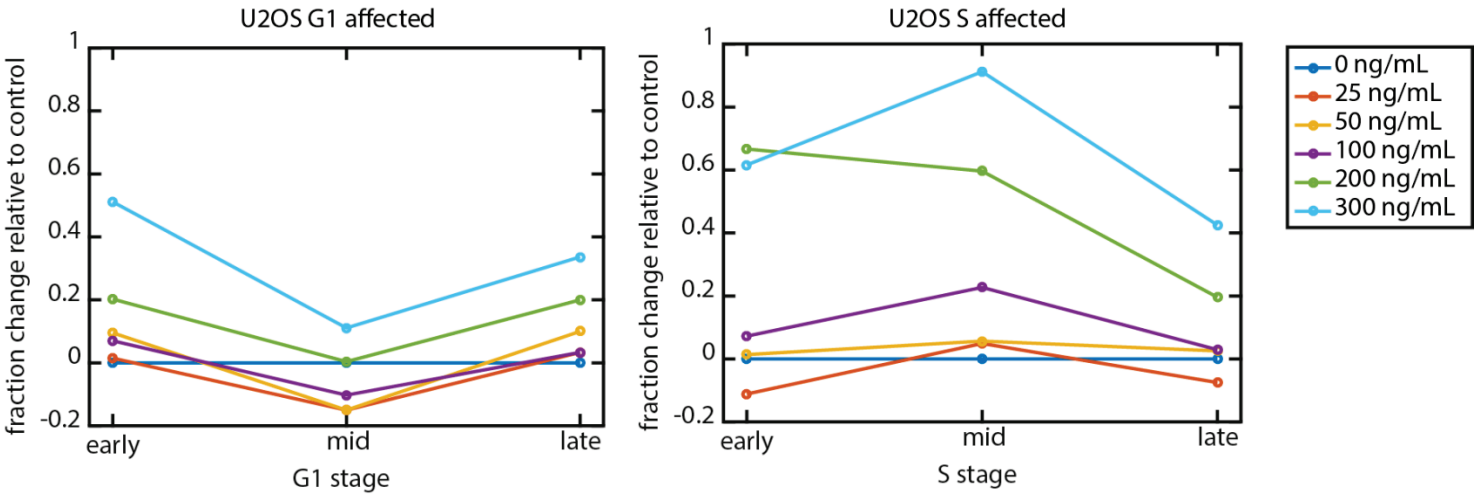

Figure S16. Cell cycle outcomes in response to DSBs depend on cell cycle phases and stages within each phase.

Cell cycle outcome's dependency on the stage of cell cycle phase progression, as in **Figure 6F**. Cell cycle outcomes are plotted as a function of cell cycle phase stage—early, mid, and late stages. Early, mid, and late stages were categorized based on thresholds defined by the 33 and 67 percentiles of time spent in a phase at the time of damage. We could not construct such cell cycle phase stage plot in RPE's G2/M due to the short length of G2/M duration and sparsity of cell (see **Figure S13E**). The increased affected fraction in late G1 stage can be explained by sampling bias, such that cells categorized as the late stage were possibly already activating arrest response before NCS treatment. Therefore, there is a strong dependency of total duration on the stage during which the cell is sampled, as seen in Figure S12B left panel.

bioRxiv preprint doi: https://doi.org/10.1101/137307; this version posted May 12, 2017. The copyright holder for this preprint (which was not certified by peer review) is the author/funder, who has granted bioRxiv a license to display the preprint in perpetuity. It is made available under aCC-BY 4.0 International license.

Table 1. Fitting parameters for the "arrest-and-restart" checkpoint model.

G1			
	NCS (ng/mL)	**time delay (h)**	**permanent arrest probability**
RPE	0	0.4932	0.0252
	10	1.8399	0.2147
	25	1.7891	0.2333
	50	0.0864	0.4596
	100	0.1242	0.6717
U2OS	0	0.7872	0.0221
	25	0.075	0.0738
	50	1.3993	0.0611
	100	0.4638	0.0553
	200	9.31E-01	0.2281
	300	0.9816	0.311
S			
	NCS (ng/mL)	**time delay (h)**	**permanent arrest probability**
RPE	0	0.4093	0.0028
	10	0.5294	0.0042
	25	0.2848	2.96E-04
	50	0.7645	9.34E-04
	100	2.3355	0.0213
U2OS	0	3.06E-04	1.79E-04
	25	4.89E-01	5.47E-05
	50	0.5125	1.87E-04
	100	1.8002	2.49E-04
	200	2.2	0.0099
	300	6.75	0.0093
G2M			
	NCS (ng/mL)	**time delay (h)**	**permanent arrest probability**
RPE	0	0.3022	3.59E-04
	10	1.0622	0.0456
	25	2.1987	0.1081
	50	5.0812	0.5414
	100	4.9552	0.7361
U2OS	0	4.98E-01	0.0104
	25	1.6519	0.0105
	50	3.4003	0.0112
	100	6.5444	0.0726
	200	9.3505	0.1656
	300	0.9816	0.311

bioRxiv preprint doi: https://doi.org/10.1101/137307; this version posted May 12, 2017. The copyright holder for this preprint (which was not certified by peer review) is the author/funder, who has granted bioRxiv a license to display the preprint in perpetuity. It is made available under aCC-BY 4.0 International license.

Table S2. Fitting parameters for the refined checkpoint model with all-or-none kinetics.

G1					
	NCS	**time delay (h)**	**permanent arrest probability**	**commitment point (fraction from phase onset)**	**difference between data and model**
	0	0.5059	0.0592	0.6047	0.074
	10	8.7336	0.2941	0.5104	0.2291
	25	8.8012	0.3824	0.5084	0.3027
	50	16.5	0.72	0.52	0.0547
RPE	**100**	22.0196	0.818	0.7484	0.0351
	0	5.29E-01	2.13E-05	0.9496	0.1222
	25	9.04E-05	0.0993	0.6333	0.0542
	50	2.2204	0.0922	0.6758	0.1748
	100	0.9751	0.1489	0.3506	0.0933
	200	4.00E+00	0.4	0.5139	0.0879
U2OS	**300**	7.8327	0.5694	0.5036	0.249
S					
	NCS	**time delay (h)**	**permanent arrest probability**	**commitment point (fraction from phase onset)**	**difference between data and model**
	0	0.5988	0.0026	0.9648	0.0195
	10	0.7661	1.20E-03	0.9976	0.1123
	25	0.3742	1.40E-03	9.99E-01	3.82E-02
	50	0.6504	1.40E-03	9.98E-01	2.82E-02
RPE	**100**	2.3799	9.54E-04	0.9974	0.52
	0	2.23E-05	1.89E-05	0.7009	0.0823
	25	1.05E+00	8.77E-20	1.00E+00	3.98E-02
	50	8.42E-08	1.01E-02	0.0967	0.016
	100	1.9833	1.53E-04	0.8988	0.0371
	200	4.0074	0.04	0.4002	0.1035
U2OS	**300**	8.5809	0.031	0.897	0.1367
G2M					
	NCS	**time delay (h)**	**permanent arrest probability**	**commitment point (fraction from phase onset)**	**difference between data and model**
	0	0.2606	1.40E-03	0.7178	0.0258
	10	1.45	0.0543	0.7621	0.0723
	25	2.294	0.121	0.9057	0.0667
	50	6.0419	0.651	0.8184	0.0642
RPE	**100**	6	0.81	0.88	0.0551
	0	1.05E+00	2.50E-04	0.9995	0.0932
	25	1.9333	9.70E-03	8.53E-01	0.0547
	50	3.2045	1.00E-02	0.8774	0.0575
	100	6.58	0.0731	0.9554	0.0706
	200	9.3695	0.178	0.9573	0.0554
U2OS	**300**	15.1824	0.5423	0.9587	0.0308

bioRxiv preprint doi: https://doi.org/10.1101/137307; this version posted May 12, 2017. The copyright holder for this preprint (which was not certified by peer review) is the author/funder, who has granted bioRxiv a license to display the preprint in perpetuity. It is made available under aCC-BY 4.0 International license.

Table S3. Fitting parameters for the refined checkpoint model with graded slowdown kinetics.

G1					
	NCS	**slowdown factor**	**permanent arrest probability**	**commitment point (fraction from phase onset)**	**difference between data and model**
RPE	**0**	0.952	0.0191	0.9999	0.0487
	10	0.5832	0.157	0.9581	0.2804
	25	0.5795	0.2008	0.9998	0.1297
	50	0.2573	0.6969	0.594	0.0868
	100	0.3313	0.7971	0.7878	0.076
U2OS	**0**	0.71	1.25E-04	0.9999	0.1167
	25	0.1112	0.194	0.0989	0.0425
	50	0.5121	0.047	0.8961	0.0487
	100	0.2093	2.95E-01	0.0978	0.039
	200	6.80E-01	0.2175	0.9999	0.0479
	300	0.51	0.288	0.9998	0.1006
S					
	NCS	**slowdown factor**	**permanent arrest probability**	**commitment point (fraction from phase onset)**	**difference between data and model**
RPE	**0**	0.95	2.30E-04	0.9699	0.0362
	10	0.9077	9.21E-05	0.9705	0.2602
	25	0.9061	2.50E-04	9.70E-01	6.66E-02
	50	0.9059	2.70E-04	9.70E-01	2.51E-02
	100	0.5971	3.76E-04	0.9614	0.119
U2OS	**0**	0.9022	2.50E-04	0.1015	0.1106
	25	0.9	5.72E-08	1.00E+00	5.48E-02
	50	0.9015	5.84E-05	0.8971	0.0202
	100	0.8076	4.48E-07	0.9	0.0695
	200	0.6952	1.49E-05	0.9998	0.0826
	300	0.3823	3.34E-04	0.9997	0.1123
G2M					
	NCS	**slowdown factor**	**permanent arrest probability**	**commitment point (fraction from phase onset)**	**difference between data and model**
RPE	**0**	0.9042	1.25E-05	0.99	0.0284
	10	0.6929	0.0599	0.9488	0.1943
	25	0.5034	0.104	0.9999	0.1751
	50	0.2945	0.6061	0.8974	0.1301
	100	0.2855	0.8166	0.8792	0.0631
U2OS	**0**	0.7979	2.59E-04	0.9999	0.2536
	25	0.604	2.08E-04	0.9023	0.043
	50	0.4904	1.44E-04	1.00E+00	0.1152
	100	0.3144	0.0292	0.8998	0.5278
	200	0.3103	0.1499	1	0.9916
	300	0.0994	0.25	1	0.3046